

I give permission for public access to my thesis and for any copying to be done at the discretion of the archives librarian and/or the College Librarian

---

Amy Cora Dubuc

---

05/11/08

# CONFORMATIONAL CHANGE INDUCED IN A RANDOM COIL PEPTIDE BY PRION PEPTIDE AGGREGATES

**Amy Cora Dubuc**

**A thesis submitted to the faculty of Mount Holyoke College in  
partial fulfillment for the degree of Bachelor of Arts with Honors**

**Department of Chemistry  
Mount Holyoke College  
South Hadley, Massachusetts  
May 2008**

## ACKNOWLEDGEMENTS

This thesis was prepared under the direction of Professor Sean M. Decatur for eight credits of independent research.

I would like to thank Professor Decatur for his continual guidance and support. He is a remarkable person who has taught us all so much, and it is truly a great loss to Mount Holyoke that he is leaving.

I would also like to thank Angela Pozo Ramajo and Kalani Seu for their endless patience with my many, many questions and their much-appreciated feedback on my symposium presentation and thesis drafts.

I am also grateful for the love and support offered by my family, fiancé, and friends. Without their constant encouragement I would never have made it this far. Their optimism is what made the journey so wonderful.

Finally, I would like to thank Jeff Knight and Maria Gomez for agreeing to be on my thesis committee. They are both such wonderful people; I have learned a great deal from them over the past four years and am grateful for the kindness they have shown me along the way.

## Abstract

In order for a protein to perform its normal function, it must adopt its native structure through proper folding. Improper folding can result in protein aggregation, which is associated with many human disorders such as Type II diabetes, Parkinson's and Alzheimer's diseases. Aggregation can be harmful because there is not only a loss of properly functioning proteins but also toxicity from the aggregate species.<sup>1</sup>

Due to the difficulty of studying the folding and aggregation of large proteins, peptides that are derived from natural sequences are common model systems for understanding aggregates.<sup>2</sup> The prion protein PrP<sup>C</sup> is one such protein that can misfold and aggregate, resulting in disease. Studying the H1 peptide, which is the most amyloidogenic region of PrP<sup>C</sup> (residues 109-122, Ac-MKHMAGAAAAGAVV-NH<sub>2</sub>), can provide useful information about misfolding and aggregation. Stable amyloid fibers form only after H1 adopts its anti-parallel  $\beta$ -sheet conformation with residue 117 aligned across all of the strands. Substitutions that prevent the peptide from adopting the ordered alignment disrupt the formation of stable  $\beta$ -sheet and prevent aggregation.<sup>3</sup> One example of a disruptive mutation is H19G (PrP A117G), in which the ninth residue of the H1 peptide (residue 117 in the prion protein) is changed from alanine to glycine. The glycine mutation disrupts  $\beta$ -sheet formation by introducing flexibility into the peptide backbone. As a result, A117G exists almost entirely in its monomeric, random coil form.

In this experiment, H19G was mixed with standard H1 and monitored by IR as a function of time and temperature. In the presence of H1, H19G changed conformation to form  $\beta$ -sheet. The kinetics and mechanism of the reaction were studied in detail, and data suggest that H1 peptides serve as a template, or "seed," for the assembly of H19G aggregates. The mechanism of the reaction was further investigated through the use of isotope-edited FTIR. After labeling residue 117 of H1 with <sup>13</sup>C, the observed loss of transition dipole coupling revealed that the new  $\beta$ -sheet was formed with H1 and H19G alternating every other strand.

---

<sup>1</sup> Chiti, F.; Taddei, N.; Baroni, F.; Capanni, C.; Stefani, M.; Ramponi, G.; Dobson, C. *Nat. Struct. Biol.* 2002, 9, 137.

<sup>2</sup> Silva, R. A.; Barber-Armstrong, W.; Decatur, S. *J. Am. Chem. Soc.* 2003, 125, 13674.

<sup>3</sup> Petty, S. A.; Adalsteinsson, T.; Decatur, S. *Biochemistry* 2005, 44, 4720.

## Table of Contents

Title Page.....	i
Acknowledgements.....	ii
Abstract.....	iii
Table of Contents.....	iv
List of Figures.....	v
List of Tables.....	vi
<b>I. Introduction.....</b>	<b>1</b>
Protein folding and Misfolding.....	1
Using Energy Landscapes to Visualize Protein Folding and Aggregation.....	5
Aggregation and Amyloid Formation.....	8
Using Infrared Spectroscopy to Study Protein Structure.....	12
The Prion Protein PrP and the H1 Peptide.....	15
Mixing Variants of the H1 Peptide.....	18
<b>II. Materials and Methods.....</b>	<b>20</b>
Peptide Synthesis.....	20
Processing of Peptides.....	23
IR Preparation.....	23
IR Measurements- Temperature Dependence of Peptides.....	24
IR Measurements- Temperature Dependence of Peptide Mixtures.....	24
IR Measurements- Time and Temperature Dependence of Peptide Mixtures.....	25
Processing of IR Spectra.....	25
<b>III. Results.....</b>	<b>27</b>
Processing of Peptides.....	27
Temperature Dependence of H1, H19G, and H1/H19G Mixtures.....	29
Time and Temperature Dependence of the H1/H19G Peptide Mixtures.....	38
Temperature Dependence of H1, H19G*, and H1/H19G* Peptide Samples.....	44
Temperature Dependence of H1*, H19G, and H1*/H19G Peptide Samples.....	48
Comparison of H1/H19G* and H1*/H19G Temperature Dependence.....	52
<b>IV. Discussion.....</b>	<b>54</b>
Processing of Peptides.....	54
Temperature Dependence of H1.....	54
The Importance of Residue 117.....	55
Temperature Dependence of H1 and H19G Mixtures.....	56
The Mechanism of the Mixing Process- Thermodynamic Control.....	58
The Mixing Process if Under Kinetic Control.....	59
Kinetics of the H1/H19G $\beta$ -Sheet Formation Suggest a General Mechanism.....	62

The Magnitude of the Activation Energy.....	64
Labeling Experiments Suggest a Specific Mechanism.....	64
Considering the Mixing Process in Greater Detail.....	69
The Mixing of H1 and H19G as a General Model for the Behavior of PrP.....	74
<b>References.....</b>	<b>77</b>

## List of Figures

### I. Introduction

Figure 1. The flexibility of the protein backbone.....	3
Figure 2. Popular models of protein folding.....	3
Figure 3. Folding funnel diagrams.....	7
Figure 4. Molecular model of an amyloid fibril.....	9
Figure 5. Schematic representations of fibril formation models.....	11
Figure 6. The amide I mode.....	12
Figure 7. Important TDC interactions in antiparallel $\beta$ -sheet.....	13
Figure 8. Characteristic amide I bands of secondary structure motifs.....	14
Figure 9. H1 $\beta$ -strands align at residue 117; aligned residues couple.....	17

### II. Materials and Methods

Figure 10. Basic steps in SPPS using Fmoc chemistry.....	22
--	----

### III. Results

Figure 11. Chromatogram and mass spectrum for H1.....	28
Figure 12. IR absorbance spectrum for the concentrated H1 solution.....	31
Figure 13. IR absorbance spectrum for the dilute H19G solution.....	31
Figure 14. Average of concentrated H1 and dilute H19G spectra.....	32
Figure 15. IR spectra for the concentrated H1/ dilute H19G mixture.....	32
Figure 16. IR absorbance spectrum for the dilute H1 solution.....	35
Figure 17. IR absorbance spectrum for the concentration H19G solution.....	35
Figure 18. Average of dilute H1 and concentrated H19G spectra.....	36
Figure 19. IR spectra for the dilute H1/ concentrated H19G mixture.....	36
Figure 20. Initial and final 25 °C spectra for concentrated H1/ dilute H19G.....	37
Figure 21. Initial and final 25 °C spectra for dilute H1/ concentrated H19G.....	37
Figure 22. Time and temperature dependence of the H1/H19G mixture.....	39
Figure 23. Normalized kinetics plots for H1/H19G at 25, 35, and 45 °C.....	41
Figure 24. Arrhenius plot for $T_1$ of the H1/H19G mixture.....	43
Figure 25. IR absorbance spectrum for the H1 peptide.....	46
Figure 26. IR absorbance spectrum for H19G*.....	46
Figure 27. Average of H1 and H19G* spectra.....	47

Figure 28. IR spectra for the H1/H19G* mixture.....	47
Figure 29. IR absorbance spectrum for H1*.....	50
Figure 30. IR absorbance spectrum for H19G.....	50
Figure 31. Average of H1* and H19G spectra.....	51
Figure 32. IR spectra for the H1*/H19G mixture.....	51
Figure 33. Difference spectra for the H1/H19G* mixture.....	53
Figure 34. Difference spectra for the H1*/H19G mixture.....	53

#### **IV. Discussion**

Figure 35. Reaction coordinate for a kinetically controlled process.....	60
Figure 36. General mechanism for the incorporation of H19G into H1 $\beta$ -sheet...67	67
Figure 37. Adjacent $\beta$ -strands are held together by hydrogen bonds.....	70
Figure 38. Mechanism for the alignment of the H1 peptide.....	71
Figure 39. Specific mechanism for the incorporation of H19G into H1 $\beta$ -sheet...73	73
Figure 40. PrP <sup>Sc</sup> induces the conformational conversion of PrP <sup>C</sup> .....	74

#### **List of Tables**

##### **II. Materials and Methods**

Table I. Peptides used in this study.....	26
---	----

##### **III. Results**

Table II. Concentration of ACN required for elution.....	27
--	----

## **I. Introduction**

### *Protein Folding and Misfolding*

The early nineteenth century featured the discovery of a class of molecules that were recognized to be of such great importance that they were given the Greek name “proteins,” meaning “standing in front” or “in the lead.”<sup>1</sup> Proteins carry out the duties encoded in genetic information and are said to generate biological activity.<sup>2,3</sup> They are involved in many diverse functions, including catalysis, cell signaling, structural scaffolding, DNA replication, and regulation of cellular growth and differentiation.

To perform its function, each protein must assume a distinct three-dimensional structure that allows it to interact with another molecule in a very specific way. When a protein fails to adopt and retain its native structure, a wide range of diseases can result. The immense importance of proteins has been recognized, making protein biochemistry a subject of intense research. However, much remains unknown about the connections between protein misfolding and its ability to cause disease.

Pioneering work in protein folding was performed in 1973 by Christian Anfinsen, who considered the connection between a protein’s amino acid sequence and its biologically active conformation. His thermodynamic hypothesis proposed that the native three-dimensional structure of a protein in its normal physiological environment would be that which allowed for the system to exist at its lowest Gibbs free energy. To assign relative energies, this hypothesis

considers the sum of all interactions in the system, which are dependent on the protein's amino acid sequence. Anfinsen also found that the three-dimensional structure of the protein was even more important than its amino acid sequence; the protein sequence could be modified significantly without losing biological function, but the macromolecular geometry must be strictly conserved.<sup>4</sup>

This work naturally suggested the question of how the protein manages to adopt this prescribed conformation. Each amino acid has two bonds that can rotate, forming phi and psi angles about the alpha carbon (Figure 1).<sup>5</sup> These angles provide the protein backbone with the flexibility it needs to be able to fold. A limited number of favored orientations can be assumed for each angle (generally two to three), but there are still an enormous number of configurations that can be adopted by the protein. A chain of  $n$  amino acids with two rotatable bonds each, where each bond has  $x$  favored orientations, can exist in  $x^{2n}$  different conformations in solution.<sup>4</sup>

A random and unbiased searching of all possible conformations would take a tremendous amount of time. Since proteins have been observed to fold on the microsecond and nanosecond scale,<sup>6</sup> it is clear there must be some other mechanism that directs protein folding. The two models that gained the most support were the framework model and the hydrophobic collapse model (Figure 2).<sup>7</sup>

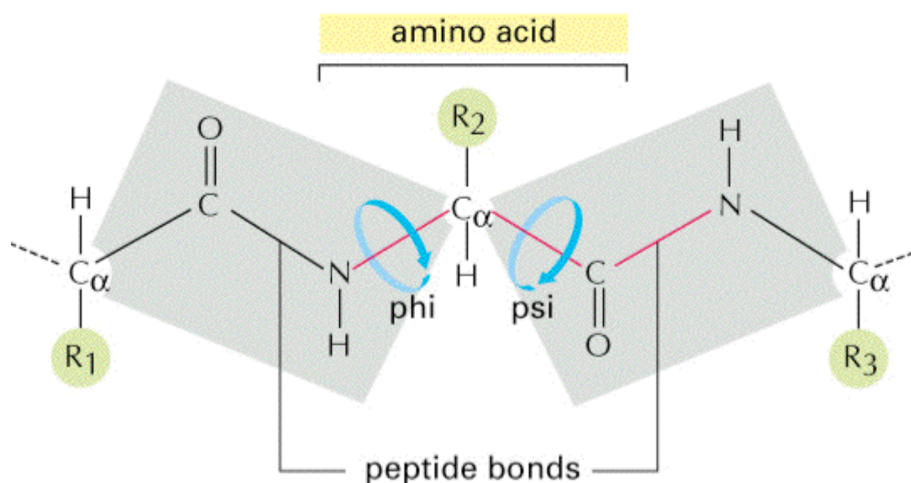


**Figure 1.** The flexibility of the protein backbone is derived from the two rotatable bonds of each alpha carbon, which generate phi and psi angles. Figure from Alberts, *et al.*<sup>5</sup>

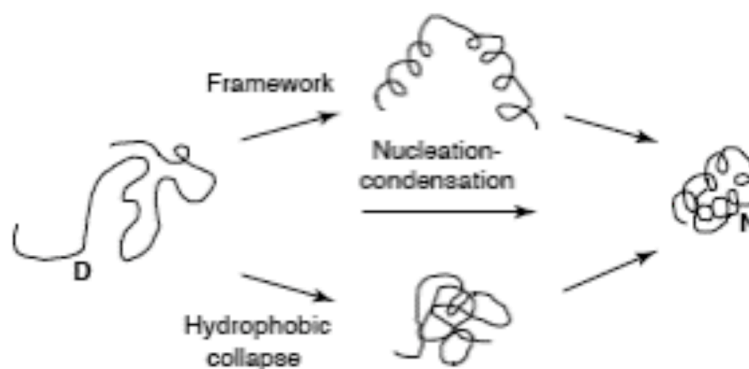


**Figure 2.** Popular models of protein folding. The framework model and the model of hydrophobic collapse are extreme situations that suggest that folding is driven by the formation of secondary structure or tertiary structure, respectively. Folding most likely occurs through a combination of these two models, through a mechanism known as nucleation-condensation that accounts for the coupling of secondary and tertiary structure formation. Figure from Daggett and Fersht, 2003.<sup>7</sup>

The framework model suggests that elements of secondary structure form first and then dock to yield the native, folded protein. In contrast, the model of hydrophobic collapse suggests that folding is driven by the expulsion of water from nearby hydrophobic residues. The protein is left in a more compact form, in which folding can proceed with fewer conformational possibilities to sample. These extreme models point to the formation of either secondary or tertiary structure as the driving force behind protein folding.

In reality, the formation of secondary structure tends to be coupled to the formation of tertiary structure. As a result, folding occurs by a mechanism that unites the framework and hydrophobic collapse models. This model is known as the nucleated-condensation model. It allows the mechanism to shift toward either extreme model with changes in the relative stability of secondary or tertiary structures.<sup>7</sup>

When proteins fold *in vivo*, the folding process is also strictly regulated by the molecular machinery of the cell. Chaperones such as Hsp60 and Hsp70 help to ensure correct folding by binding to unfolded or misfolded proteins, which gives the proteins another chance to fold properly and acts to prevent aggregation. Abnormal proteins are also tagged for destruction within the proteasome. Yet even properly folded proteins can undergo random conformational fluctuations that lead to the formation of misfolded states.<sup>8</sup>

A protein in its native state generally has hydrophilic residues located on the protein's surface, where they are exposed to the solvent, while hydrophobic

residues are hidden away in the protein's core. When a protein misfolds, some of these hydrophobic residues are inevitably exposed to the solvent. The exposure of hydrophobic residues is so energetically unfavorable that it can drive the protein to interact with other molecules in an attempt to hide these regions from the polar solvent.<sup>3</sup> When the other molecules involved are more of the same protein, the end result is aggregation, which can be defined as the interactions between multiple polypeptide chains to form a single structure.

Unsurprisingly, protein misfolding and aggregation are associated with a wide range of diseases. A misfolded and aggregated protein loses its ability to perform its biological function. Cystic fibrosis and some types of cancer are examples of the diseases that can result when a protein misfolds and is unable to function properly. There can also be a gain of toxicity from the aggregate species. Alzheimer's and Parkinson's diseases, as well as the spongiform encephalopathies and type II diabetes, are associated with the deposition and accumulation of protein aggregates in tissues such as the brain, heart, and spleen.<sup>3</sup>

### *Using Energy Landscapes to Visualize Protein Folding and Aggregation*

Energy landscapes are commonly used to describe the progression of the unfolded polypeptide down a funnel-like energy profile towards the native state (Figure 3a). The top of the funnel features all of the possible starting configurations of the unfolded chain, and the funnel's sloping sides represent the multiple routes that can be taken for the starting configuration to adopt the native

state. Intermediate states may also be populated during the process, represented by local energy minima on the energy landscape (such as  $I_A$  in Figure 3a). The polypeptide is said to be kinetically trapped in such a minimum until it has sufficient energy to overcome the barrier between the trap and the main pathway towards the native state.<sup>9</sup>

The surface of the funnel is determined by the thermodynamic and kinetic properties of the folding chain and is therefore unique for each polypeptide sequence under a given set of conditions. It is assumed that native contacts are more stable than non-native contacts; as native contacts form, the number of possible conformations is reduced and the chain is driven towards its final, native structure.<sup>8</sup> This type of funnel assumes that the percentage of polypeptide chains that misfolds is small and can be ignored.

However, proteins do misfold, so an accurate energy landscape should take this behavior into account. As described above, inappropriate interactions between partially misfolded proteins can lead to aggregation. The energy funnel in Figure 3b has been updated to account for the fact that aggregation can be a competing reaction to the correct folding process. For any given protein, it should be possible to describe the extent of aggregation with an energy funnel that considers both proper folding and aggregation. A protein in a given state (native or aggregated) could have reached this conformation because it was the most thermodynamically stable structure (with the lowest possible energy). On the other hand, the given state may only represent a local energy minimum, but it

could have a sufficiently deep kinetic trap to keep the protein in this form once it has been adopted.<sup>9</sup>

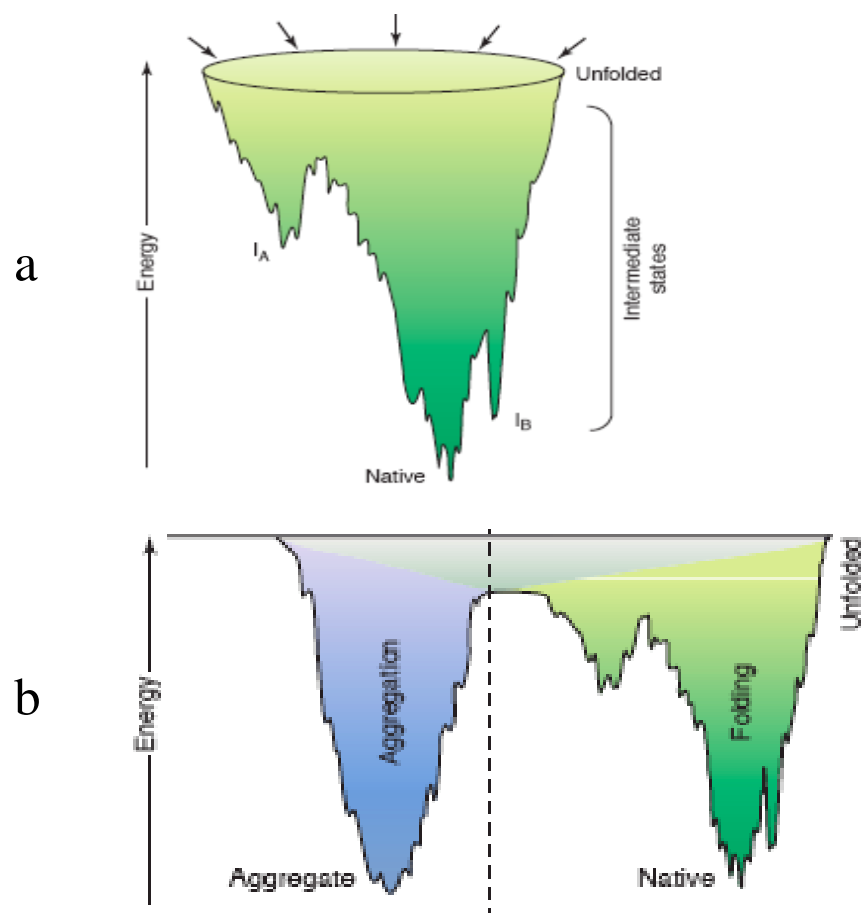


**Figure 3.** Folding funnel diagrams for (a) a “well-behaved” protein and (b) a protein for which aggregation is recognized as a competing side reaction. Figure adapted from Clark, 2004.<sup>9</sup>

### *Aggregation and Amyloid Formation*

Just as a protein has many levels of structure, there are many levels of structure that are possible in an aggregate. The first structures to form are soluble oligomers, which develop into small bead structures that are known as amorphous aggregates or micelles. These “prefibrillar aggregates” can then be transformed into species that have more defined morphologies, which are known as protofilaments or protofibrils. Fibrils can then form through lateral association of protofilaments or protofibrils, with some degree of conformational conversion.<sup>3</sup>

In particular, we can consider an amyloid, which is a general term that describes a certain class of aggregates. Amyloids are the aggregates that are associated with many human diseases known as amyloidoses, including Alzheimer’s and Parkinson’s diseases. Each disease is associated with the misfolding and aggregation (amyloid formation) of a different protein.

Comparing the proteins associated with each amyloidosis reveals little similarity in sequence, but the corresponding amyloid fibrils have many characteristics in common. All have high  $\beta$ -sheet content, are relatively insoluble, and exhibit an unexpected degree of resistance to proteolysis.<sup>10</sup> Additionally, these fibrils all have very similar morphologies, containing what is known as cross- $\beta$  structure. This type of structure features the formation of continuous  $\beta$ -sheets that are aligned perpendicular to the long axis of the fibril, as shown in Figure 4.<sup>11</sup>

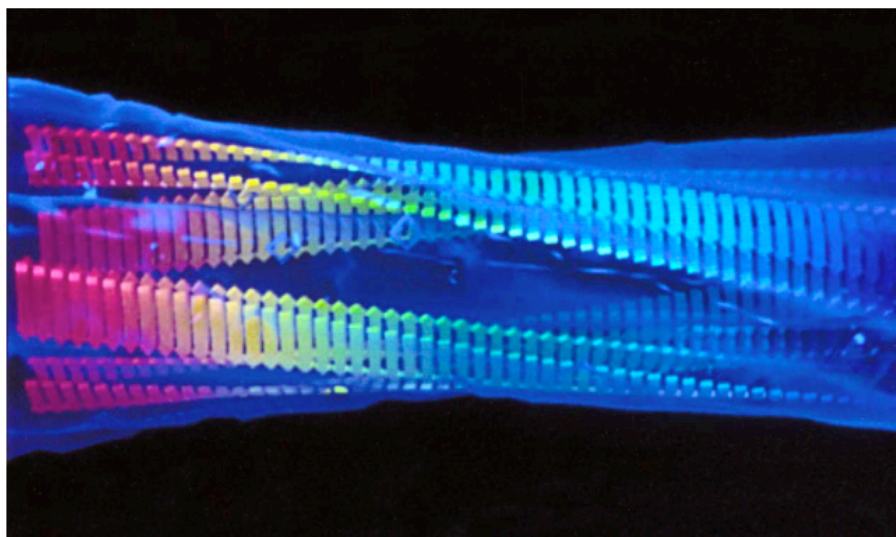


**Figure 4.** Molecular model of an amyloid fibril, featuring the characteristic cross- $\beta$  structure. The  $\beta$ -sheets are aligned perpendicular to the axis of the fibril. Figure from Dobson, 2004.<sup>11</sup>

Many models have been proposed to describe the mechanism of amyloid formation. The three most popular are templated assembly, monomer-directed conversion, and nucleated polymerization, as presented in Figure 5.<sup>12</sup>

The model of templated assembly (Figure 5a) describes amyloid formation as the binding of a soluble state (S) random coil monomer to a preassembled nucleus in a quick pre-equilibrium step, followed by the incorporation of the monomeric peptide onto the growing end of the fibril in the rate-determining step.

The monomer-directed conversion (MDC) model (Figure 5b) suggests that a monomeric peptide can adopt a conformation (A) that is similar to that adopted when in the fibril. The rate-determining step in this model is the binding of an A-state monomer to an S-state monomer. This changes the conformation of the S-state monomer, such that the end result is an A-state dimer. The dimer can then dissociate, and the two A-state monomers can be incorporated into the fibril.

Nucleated polymerization (NP, Figure 5c) is a commonly used model that is similar to crystallization. This mechanism stipulates that there is an equilibrium between the S- and A-state monomers, with the S-state heavily favored. This equilibrium allows for the rate-limiting and unfavorable formation of an A-state nucleus. Once a nucleus has been formed, however, A-state monomers can readily be added to the growing end of the fibril (nucleus).

One model is likely insufficient to describe amyloidogenesis for all proteins. Different proteins likely aggregate via different mechanisms; some

might require combinations of the abovementioned models or a different model altogether.

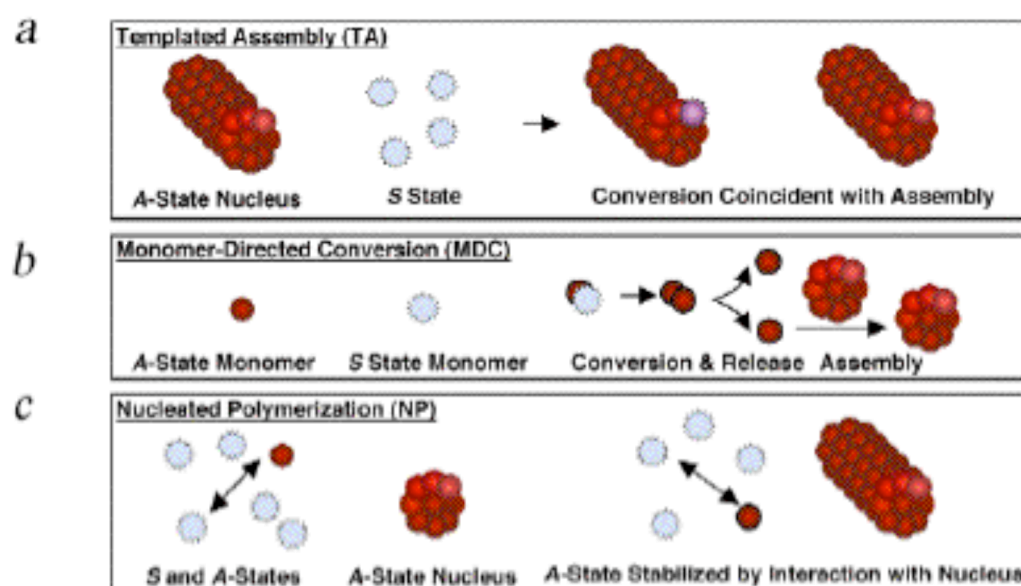


**Figure 5.** Schematic representations of the three popular models of fibril formation: templated assembly (a), monomer-directed conversion (b), nucleated polymerization (c). Figure from Kelly.<sup>12</sup>

### *Using Infrared Spectroscopy to Study Protein Structure*

Infrared radiation can be absorbed by a molecular vibration when the energy of a photon of infrared radiation ( $E = h\nu$ ) exactly matches the difference in energy between two adjacent vibrational energy levels. Each molecular vibration can be modeled as a simple harmonic oscillator. The frequency of oscillation can then be given by

$$\nu = \frac{1}{2\pi} \sqrt{\frac{k}{\mu}} \quad (1)$$

where  $\mu$  is the reduced mass and  $k$  is the force constant of the “spring” connecting the two atoms. Each vibrational mode produces an absorbance peak in the protein’s IR spectrum at the frequency of light that is absorbed. One particularly useful vibration is the amide I mode, which arises mainly from the stretching of the backbone carbonyl (illustrated in Figure 6) and produces a band in the IR spectrum between 1600 and 1700  $\text{cm}^{-1}$ .<sup>13,14</sup>

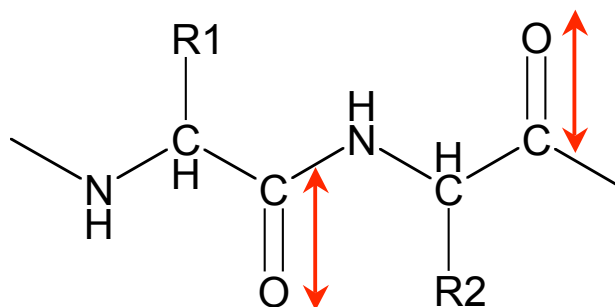


**Figure 6.** The stretching of the backbone carbonyl generates the amide I mode (1600-1700  $\text{cm}^{-1}$ ) in the IR spectrum of a polypeptide.

Coupling of the amide I modes provides information about the secondary structure of the peptide. Amide I modes can couple in several ways, but the most important form of coupling is transition dipole coupling (TDC). TDC is a through-space coulombic interaction between certain neighboring amide I modes, as shown in Figure 7. It occurs to an extent that is determined by the relative positions of the coupled oscillators, which in turn are affected by the configuration of the peptide backbone. Each type of secondary structure is therefore characterized by a specific backbone configuration, amount of transition dipole coupling (TDC), and vibrational frequency.

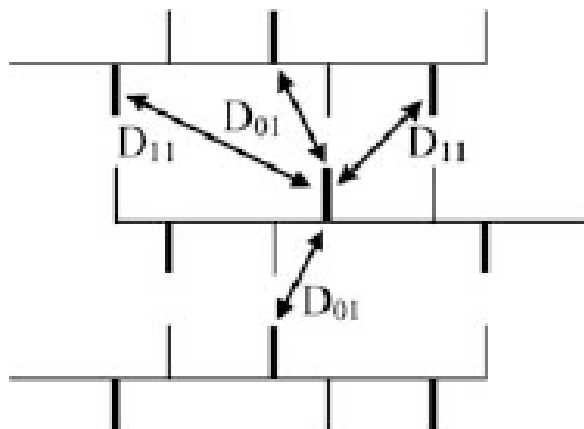


**Figure 7.** Antiparallel  $\beta$ -sheet with the backbone carbonyls shown in bold. The most significant transition dipole coupling occurs between the carbonyl neighbors connected by arrows. Figure from Barth and Zscherp, 2002.<sup>13</sup>

As a result, IR spectroscopy is very sensitive to the protein's secondary structure. The characteristic signals produced by each type of secondary structure are presented in Figure 8.<sup>13,14</sup>  $\alpha$ -helix structure produces a band at  $1630\text{ cm}^{-1}$ , antiparallel  $\beta$ -sheet produces two bands at  $1690$  and  $1620\text{ cm}^{-1}$ , and random coil produces a band around  $1650\text{ cm}^{-1}$ .

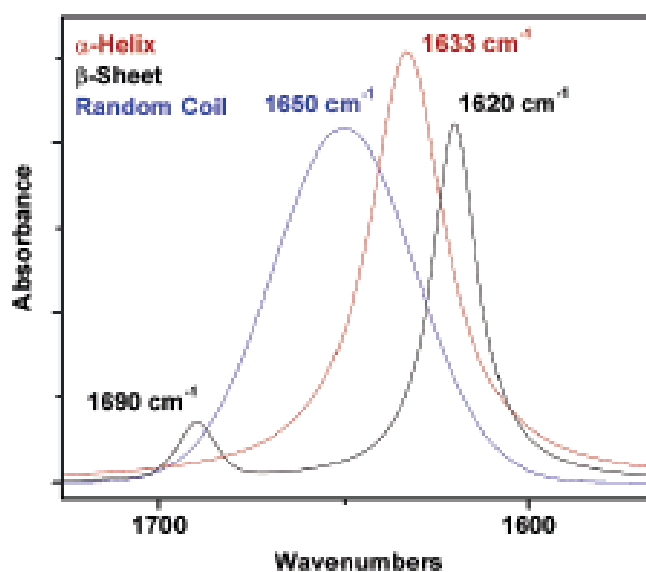


**Figure 8.** The amide I bands generated by  $\alpha$ -helix,  $\beta$ -sheet, and random coil secondary structure. Figure from Decatur, 2006.<sup>14</sup>

The IR absorbance spectrum readily provides information about the protein's secondary structure, but IR spectroscopy can also be used to gain insight into residue-level structure and dynamics. Since the frequency of vibrations is dependent on the reduced mass of the oscillator (Equation 1), it is possible to

change the frequency of the amide I vibration by labeling the backbone carbonyl. Specifically, labeling the backbone carbonyl with  $^{13}\text{C}$  (increasing the reduced mass) decreases the frequency of vibrations and produces a shoulder to the main amide I band at lower wavenumbers.<sup>14</sup>

This method of isotope-edited infrared spectroscopy has been successfully applied to characterize the structure and behavior of a short peptide that was derived from the Syrian hamster prion protein, as described below.

#### *The Prion Protein PrP and the H1 Peptide*

The misfolding and aggregation of the PrP<sup>Sc</sup> isoform of cellular prion protein (PrP<sup>C</sup>) are associated with a class of prion diseases known as the transmissible spongiform encephalopathies (TSEs). Due to their large size and dynamic nature, it is difficult to isolate and characterize the aggregated species of many proteins. Instead, many scientists study the aggregation process using small, amyloidogenic peptides that are derived from the full-length protein of interest. To this end, the most amyloidogenic sequence of the prion protein (residues 109-122) has been reproduced in the form of the H1 peptide.<sup>15,16,17</sup> Studying the folding and aggregation of the H1 peptide can provide insight into the folding and aggregation processes of the full-length, infectious prion protein.

The H1 peptide has been characterized in detail using standard and isotope-edited IR spectroscopy. IR absorbance spectra of H1 reveal that strands of this peptide aggregate to form antiparallel  $\beta$ -sheet structure. Labeling the

backbone carbonyl of any residue with  $^{13}\text{C}$  produced a shoulder to the main amide I band, as was expected. However, sequentially labeling each residue revealed that residue 117 was unique. When this residue was labeled, the  $^{13}\text{C}$  band appeared in the IR spectrum to the right of the main amide I band and then shifted towards lower wavenumbers (from 1600 to 1590  $\text{cm}^{-1}$ ) as the temperature was increased.<sup>17</sup>

This shift in frequency can be attributed to an altered coupling with neighboring amide I oscillators.<sup>13</sup> It was suggested that the H1 peptide initially forms a disordered  $\beta$ -sheet that later rearranges to a configuration that has residue 117 aligned across all  $\beta$ -strands, as shown in Figure 9. As the strands come into alignment, the labeled residues at position 117 are brought closer to one another and are able to couple to a greater extent. The change in coupling results in the observed shift in the frequency of the  $^{13}\text{C}$ -labeled amide I mode.<sup>17</sup>

Additional studies further emphasized the importance of residue 117. The secondary structure was determined for a series of H1 variants that were mutated at residue 117, and for each mutant, the labeling experiment was performed as described above. AFM imaging was also used to characterize aggregate morphology. The results of this study revealed that the side chain at residue 117 had an enormous impact on the overall secondary structure and aggregate morphology of the peptide. The standard H1 peptide was shown to form twisted fibrils, but only after the  $\beta$ -strands had come into alignment at residue 117.

Furthermore, mutants that were able to align at position 117 still formed twisted fibrils, but other alignments produced only thin protofibrils.<sup>16</sup>

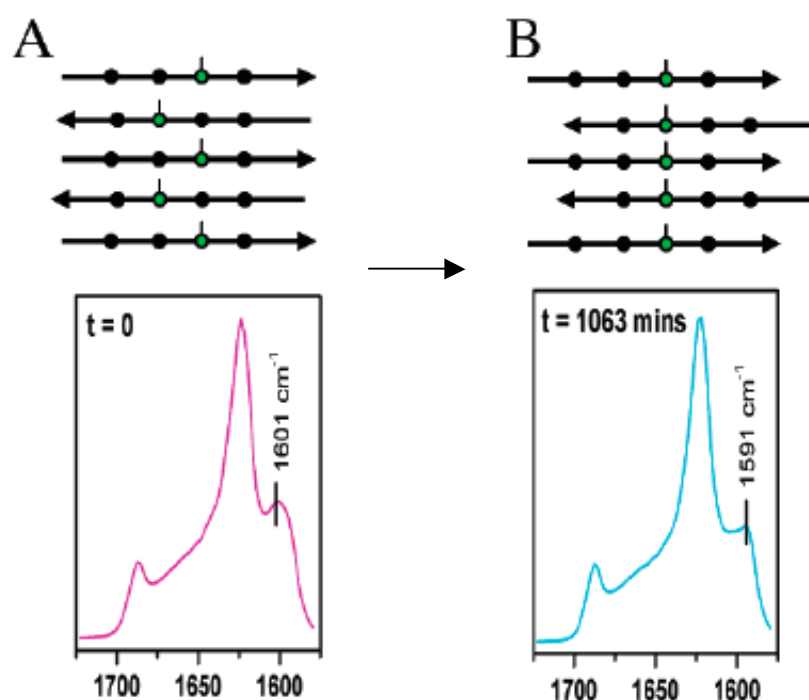


**Figure 9.** The H1  $\beta$ -strands undergo a gradual shift from an initial disordered conformation (a) to adopt a conformation that has residue 117 (green) aligned across all strands (b). The  $^{13}\text{C}$ -labeled amide I band shifts to lower wavenumbers during this process. Figure adapted from Decatur, 2006.<sup>14</sup>

### *Mixing Variants of the H1 Peptide*

This study sought to determine what would happen if the standard H1 peptide was mixed with the H19G mutant. This mutation substitutes a glycine for an alanine at the important 117 (PrP) position. As a result, the H19G peptide has a much more flexible peptide backbone, which destabilizes the formation of  $\beta$ -sheet; the peptide exists almost entirely as random coil.<sup>16</sup>

In other words, this study was performed to characterize the mixture that resulted from mixing a  $\beta$ -sheet peptide (H1) with a random coil peptide (H19G). Standard IR spectroscopy was used to gain information about the secondary structure of the mixture, and isotope-edited IR spectroscopy provided information about the mechanism of the mixing process. Results from these experiments provided a wealth of data that were analyzed in light of the models of fibril formation presented above (Figure 5) to gain insight into the mechanism of the H1 and H19G mixing process.

Analyzing the interactions between variants of a peptide could be instructive in the event that a biological system had only some fraction of its peptide population mutated. This could occur if only one copy of a gene were altered, such that the two resulting gene forms produced two peptide variants. It is also possible to introduce an external source of protein (through ingestion, for example) that differs slightly from the host's version of the same protein. In such a case, it is clear that we would want to understand what happens when protein

variants mix. To accomplish this, we turn to mixtures of our model peptide variants.

## II. Materials and Methods

### *Peptide Synthesis*

The H1 peptide (PrP 109-122) and variants (see Table I) were synthesized using standard Fmoc ( $N^{\alpha}$ -9-fluorenylmethyloxycarbonyl) chemistry on a Liberty peptide synthesizer.<sup>18</sup> See Figure 10 for an overview of the basic steps involved in solid phase peptide synthesis (SPPS) using Fmoc chemistry.

SPPS is performed by coupling amino acids to insoluble resin beads (Fmoc-PAL-PEG-PS) that are present in the reaction mixture, extending the peptide from the C-terminus to the N-terminus. The resin beads were a polyethylene glycol (PEG) and polystyrene (PS) mixture, with a peptide amide-unloaded linker (PAL) used to couple the first amino acid to the resin. When performing Fmoc chemistry, the reactive amine groups on the resin and the N-terminus of each amino acid are protected with an Fmoc protecting group. Reactive side chains, such as those found on lysine and histidine, are also protected (with different protecting groups).

At the start of a synthesis, the Fmoc protecting group is removed from the resin and the first amino acid by first washing with 20% piperidine in dimethylformamide (DMF). The amino acid is activated using 2-(1H-benzotriazole-1-yl)-1,1,3,3-tetramethyluronium hexafluorophosphate (HBTU) and 1-hydroxybenzotriazole hydrate (HOBt) in DMF, which converts the carboxylic acid functional group to a more reactive ester. An activator base, N, N-Diisopropylethylamine (DIEA) in N-Methylpyrrolidone (NMP), is added to

catalyze the nucleophilic substitution reaction between the ester and the exposed amine group on the deprotected resin.

Another wash of piperidine in DMF is then performed to deprotect the new N-terminal amino acid, so that a new amino acid can be coupled to the first by using the activator and activator base as described above. This process of removing the N-terminal Fmoc group and coupling to a new protected amino acid is repeated until the desired peptide sequence has been generated.

Once the desired sequence has been constructed, the N-terminal Fmoc group is removed in the final deblocking process. The exposed N-terminus of the peptide is capped with an acetyl group using 20% acetic anhydride in DMF. A solution of 2.5% dH<sub>2</sub>O, 2.5% triisopropylsilane (TIS) in trifluoroacetic acid (TFA) is then used to cleave the peptide from the resin support and remove any side chain protecting groups. When the peptide is cleaved from the resin, it acquires an amine group on its C-terminal end that was donated by the resin's PAL linker moiety.

The resulting free peptide has an acetyl cap on its N-terminus and an amine cap on its C-terminus. These caps stabilize the ends of the peptide, which would otherwise be charged at a physiological pH. By stabilizing the termini, the structure of the peptide can more closely resemble the structure that it would have if it were embedded within the native protein from which it was derived.

### Solid Phase Peptide Synthesis Scheme

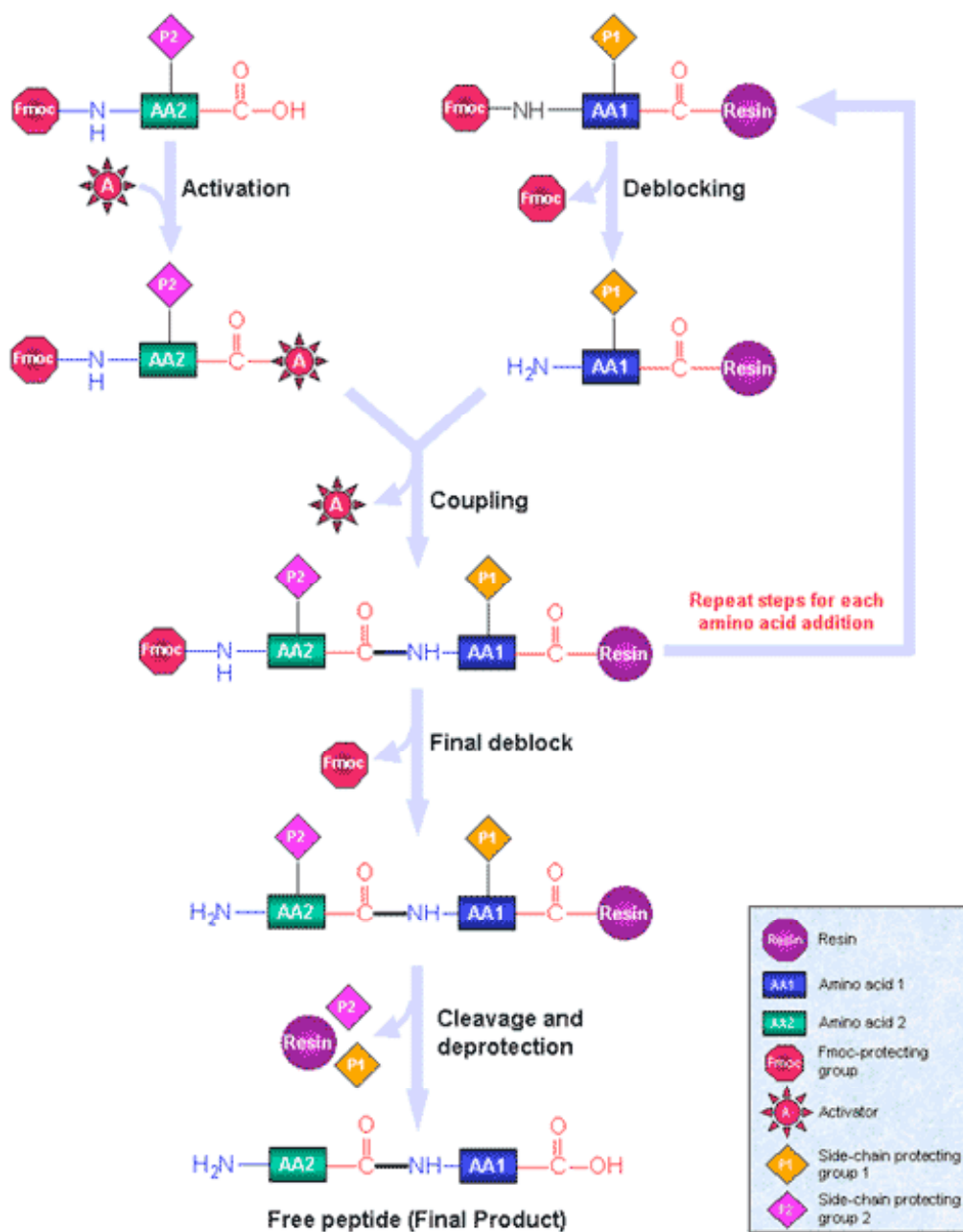


**Figure 10.** Basic steps in solid phase synthesis using Fmoc chemistry. The first amino acid is attached to the insoluble resin support, and its protecting Fmoc group is removed (deblocking). This amino acid is coupled to a second, activated and Fmoc-protected amino acid. The deprotection and coupling cycle is repeated as necessary until the desired amino acid sequence has been created. A cleavage reagent then cleaves the peptide from the resin support and removes the side chain protecting groups. Figure adapted from (19).

### *Processing of Peptides*

Peptide products were precipitated out of the cleavage cocktail by adding cold ether. The ether mixture was centrifuged at 8,000 rpm for 15 minutes to pellet the peptide. The ether was decanted, and the peptide pellet was lyophilized for 30 minutes to remove any remaining ether. The dried product was dissolved in 15 mL dH<sub>2</sub>O and 2.5 mL ACN, frozen in liquid nitrogen, and lyophilized overnight.

Peptides were purified using reverse-phase HPLC on an Amersham Pharmacia Biotech instrument with a Vydac C18 column. The mobile phase was a controlled gradient from 15 to 40 percent acetonitrile in water with trace amounts of TFA. Purified peptides were frozen in liquid nitrogen and lyophilized overnight. A sample of each peptide was sent to the mass spectrometry center at the University of Massachusetts in Amherst, and electrospray mass spectrometry (Esquire-LC\_00142) was used to verify the purity of each peptide product. Purified peptides were exchanged in 0.05 M DCl in D<sub>2</sub>O for 4 to 5 hours to remove residual TFA, because TFA absorbs IR radiation in the region of interest. Exchanged peptides were then frozen in liquid nitrogen and lyophilized overnight.

### *IR Preparation*

IR measurements were taken on a Vector22, Equinox55, or Tensor23 (Bruker) FTIR spectrometer operating at a resolution of 4 cm<sup>-1</sup>; spectra represent averages of 512 scans. Sample aliquots were placed between two CaF<sub>2</sub> windows

separated by a 100  $\mu\text{m}$  Teflon spacer, and the sample compartment was purged with nitrogen. Before all experiments, spectra of the purged chamber and of the atmospheric air were obtained for each instrument. The temperature of the cell was controlled by a water jacket connected to an external water bath.

#### *IR measurements- Temperature Dependence of Peptides*

Each peptide was dissolved in a deuterated HEPES buffer (20 mM HEPES, 100 mM NaCl, pH 7.4), vortexing and sonicating until dissolution was complete. Concentrations were unknown at the time of sample preparation, but were approximated to be 10 to 20 mg/mL. Measurements were taken at temperatures from 25 °C to 75 °C in 10 °C increments, allowing 20 minutes for the each temperature to equilibrate before scanning. The temperature was returned to 25 °C and a final measurement was taken.

#### *IR measurements- Temperature Dependence of Peptide Mixtures*

The temperature dependence of an H1/H19G mixture was studied in a similar manner. H1 and H19G were dissolved in HEPES buffer (described above), adding buffer as necessary until the viscosity and turbidity of the solutions appeared similar. The solutions were vortexed and sonicated until dissolution was complete. Exact concentrations were unknown, but were approximated to be around 10-20 mg/mL. IR spectra were recorded for each peptide individually at 25 °C. A 1:1 mixture (by volume) was prepared, vortexing

to mix. IR measurements were taken of this mixture over the temperature range 25 °C to 75 °C in 10 °C increments on a Vector22 FTIR spectrometer as described above. This process was repeated for different concentration ratios and for mixtures of H1\*/H19G and H1/H19G\*.

#### *IR measurements- Time and Temperature Dependence of Peptide Mixtures*

The temperature dependence study was expanded by simultaneously considering time and temperature as factors for the H1/H19G mixture. IR measurements were first taken of each peptide individually at 35 °C on the Vector22 spectrometer. The amide I' peak was integrated on each absorbance spectrum to obtain information about the relative concentrations of the two solutions, and the more concentrated solution was diluted as needed to make the two peptide solutions approximately equal in concentration.

A 1:1 mixture (by volume) of the two peptide solutions was prepared, vortexing to mix. IR spectra were concurrently recorded for this mixture at 25 °C on a Tensor23 spectrometer, at 35 °C on a Vector22 spectrometer, and at 45 °C on an Equinox55 spectrometer. Measurements were taken every half hour for 24 hours.

#### *Processing of IR Spectra*

All IR spectra were collected as single channel spectra using OPUS software. Files were transferred to GRAMS spectroscopy software, and a purged

air spectrum was used to convert single channel to absorbance. The single channel signal is equivalent to the raw signal detected for the peptide. By dividing this signal by the raw signal without sample (which is the spectrum of the purged sample compartment), transmittance ( $T$ ) is obtained.

$$T = \frac{\text{raw signal of peptide}}{\text{raw signal without peptide}}$$

Absorbance ( $A$ ) is then calculated using the relationship  $A = -\log T$ .

Absorbance spectra of the HEPES buffer (at the proper temperature) and of water vapor were obtained for each instrument and were subtracted from each peptide spectrum. The baseline was corrected to allow for comparisons between spectra. Absorbance spectra and kinetic curves were plotted using Origin data analysis and graphing software.

**Table I.** Peptides used in this study. An asterisk following a residue in the sequence indicates that the residue was labeled at the carbonyl with  $^{13}\text{C}$ .

Name	Sequence
H1	Ac-MKHMAGAAAAGAVV-NH <sub>2</sub>
H19G	Ac-MKHMAGAAGAGAVV-NH <sub>2</sub>
H1*	Ac-MKHMAGAAA*AGAVV-NH <sub>2</sub>
H19G*	Ac-MKHMAGAAG*AGAVV-NH <sub>2</sub>

### III. Results

#### *Processing of Peptides*

A sample HPLC chromatogram for the H1 peptide is included in Figure 11. The peptide eluted in a sharp peak at a mobile phase concentration of about 21% acetonitrile, and a lack of other similarly sized peaks reveals the relative purity of the crude sample. Table II presents the average mobile phase concentration corresponding to peptide elution for all peptides used in this project. H1 and H1\* eluted at higher concentrations of acetonitrile than H19G and H19G\*, and labeling did not seem to affect the concentration of acetonitrile required for elution.

As an example, the mass spectrum for the purified H1 peptide is also shown in Figure 11. There are two peaks at  $m/z$  values of 663.4 and 1326.6, which correspond to the doubly and singly charged peptide, respectively. The identity of the peptide was confirmed by comparing the molecular ion peak to the known molecular mass of the peptide, and its purity was verified through the lack of other peaks.

**Table II.** Average acetonitrile concentration in the mobile phase needed for elution of the peptides used in this study.

Peptide	Elution (% Acetonitrile in mobile phase)
H1	21.4
H19G	18.8
H1*	21.0
H19G*	18.7

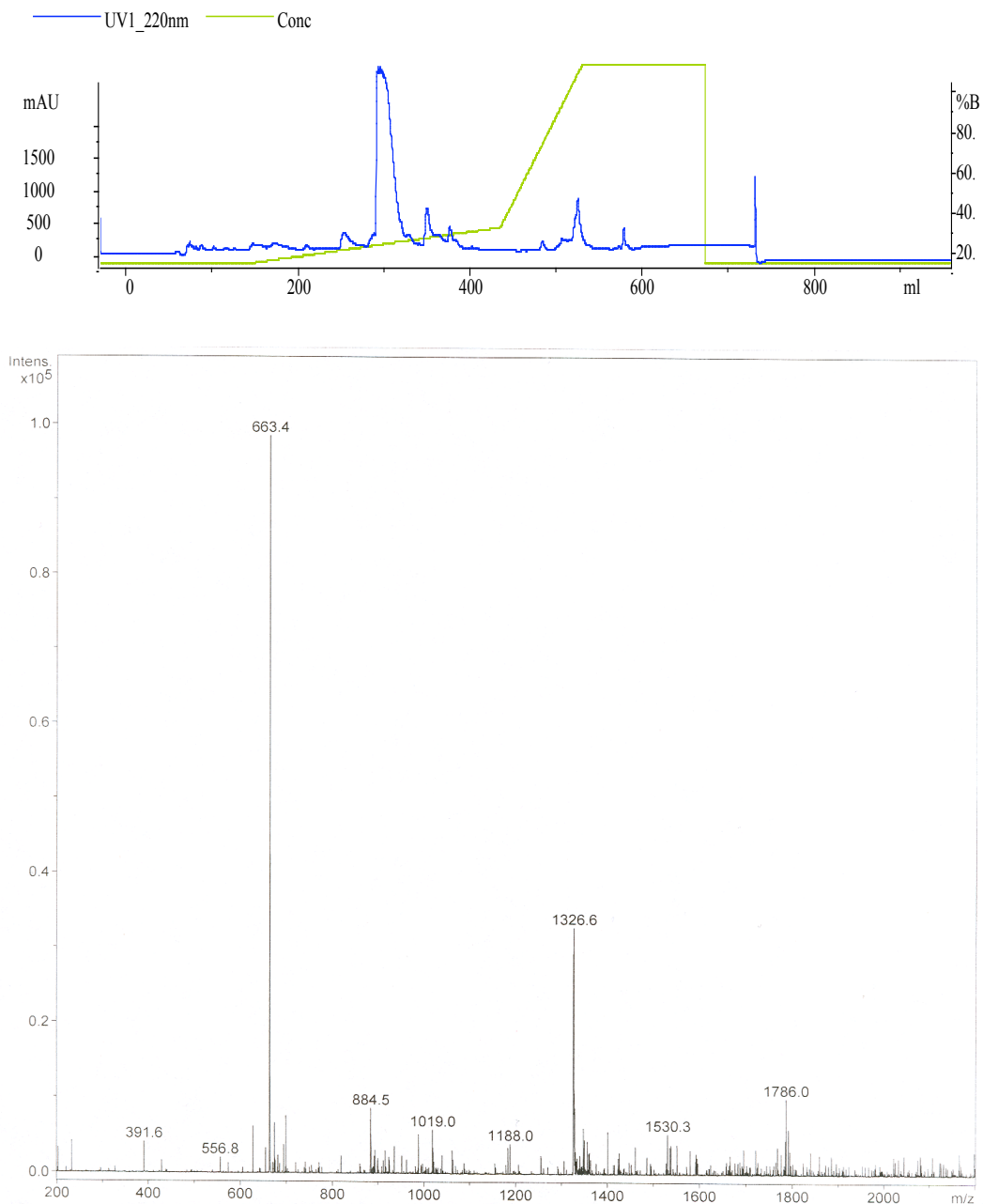


**Figure 11.** Chromatogram and mass spectrum for H1. The peptide eluted from the column in a sharp peak when the mobile phase was at a concentration of 21% acetonitrile. The mass spectrum reveals a high degree of purity; the peaks corresponding to  $m/z$  values of 663.4 and 1326.6 represent the singly and doubly charged peptide, respectively.

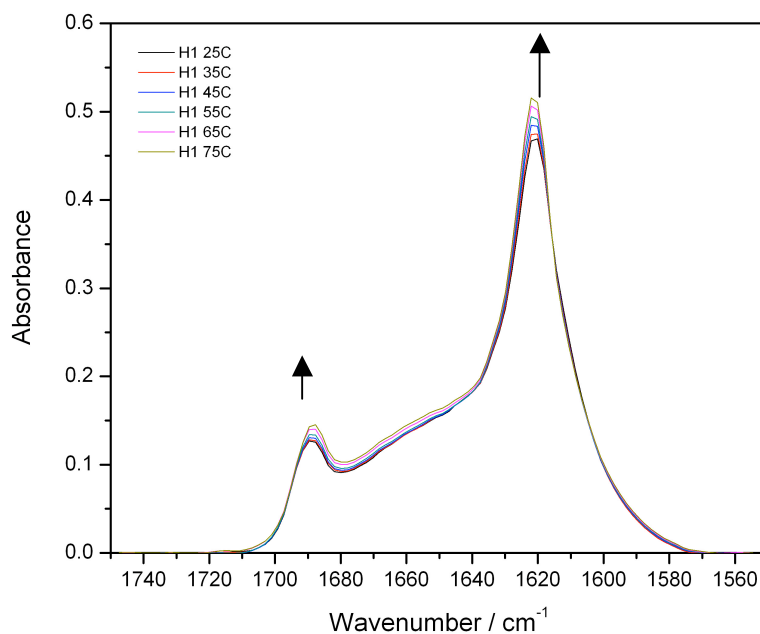
### *Temperature Dependence of H1, H19G, and H1/H19G Mixtures*

IR spectra of H1 and H19G at varying temperatures are presented in Figures 12 and 13, respectively. The H1 spectra feature the two characteristic antiparallel  $\beta$ -sheet bands at 1620 and 1690  $\text{cm}^{-1}$ , and the H19G spectra consist of a single, broad random coil band with a maximum at 1650  $\text{cm}^{-1}$ . As the temperature was increased, the H1 spectra showed a slight increase in  $\beta$ -sheet structure, and the H19G spectra showed a slight increase in random coil structure.

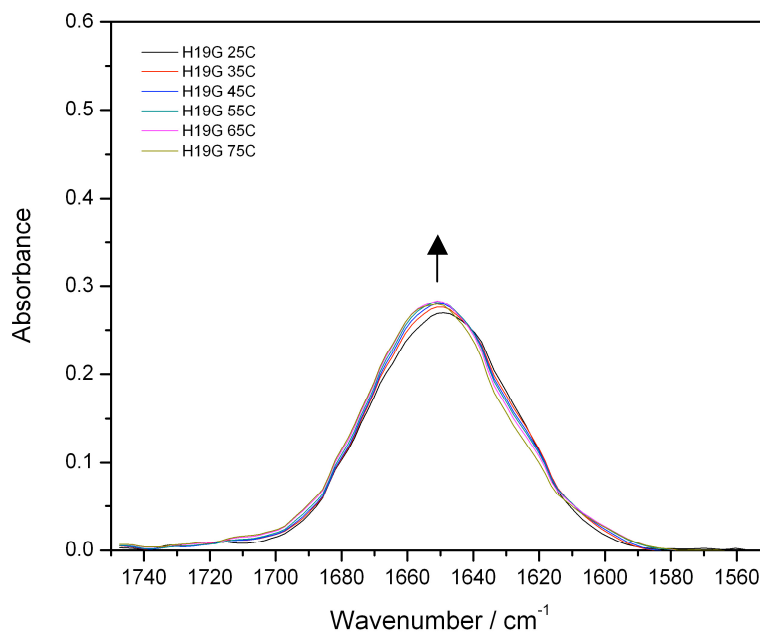
Since absorbance is proportional to concentration, integrating the absorbance of each peptide in the amide I' region provides information about the relative concentrations of each peptide solution. In this case, the H1 ( $\beta$ -sheet) solution was more concentrated than the H19G (random coil) solution, so a 1:1 (by volume) mixture of these peptide samples would have more  $\beta$ -sheet than random coil.

Figure 14 presents the spectra that would be expected of a hypothetical 1:1 (volume) mixture of the H1 and the H19G samples. To obtain these spectra, the H1 spectra (Figure 12) were added to the H19G spectra (Figure 13), and the results were divided by two. This manipulation would represent a mixture of these peptides in which the two peptides did not interact with each other. The resulting spectra described a secondary structure that was mostly  $\beta$ -sheet with some random coil, and they predicted that as the temperature increases, the amounts of both random coil and  $\beta$ -sheet should increase slightly (as monitored by increases in the bands at 1650, 1620, and 1690  $\text{cm}^{-1}$ ).

To test this prediction, a 1:1 (volume) mixture of these peptides was prepared and monitored by IR spectroscopy over a range of temperatures. The resulting IR spectra are presented in Figure 15. As predicted, the spectrum of the peptide mixture showed mostly  $\beta$ -sheet structure with some random coil, and the amount of  $\beta$ -sheet increased with increasing temperature. However, the amount of random coil structure decreased dramatically as the temperature was increased, which differed drastically from our prediction.



**Figure 12.** IR absorbance spectra for the more concentrated H1 solution. Peaks at 1620 and 1690 cm<sup>-1</sup> reveal  $\beta$ -sheet secondary structure. The amount of  $\beta$ -sheet increased with increasing temperature.



**Figure 13.** IR absorbance spectra for the more dilute H19G solution. The broad peak at 1650 cm<sup>-1</sup> reveals the presence of random coil structure, which increased in abundance as the temperature was increased.

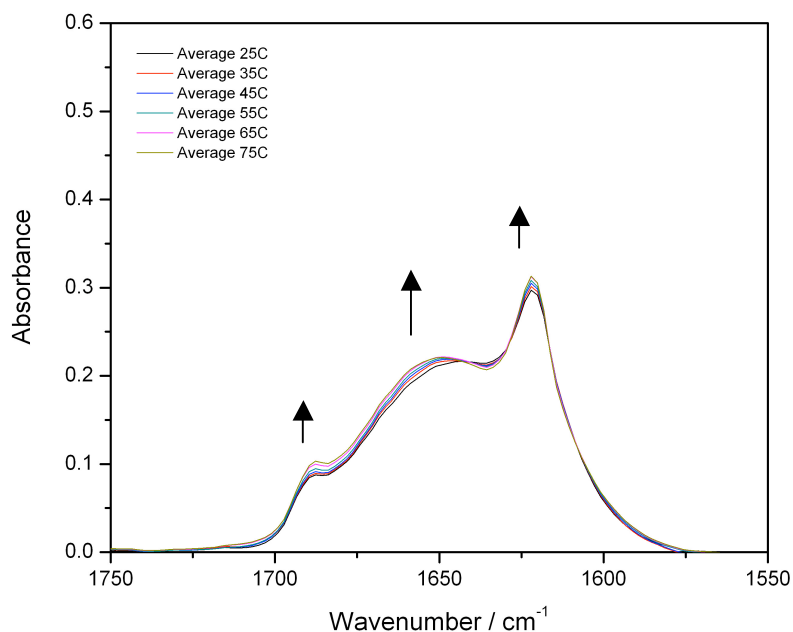


**Figure 14.** Spectra obtained by averaging spectra of concentrated H1 and dilute H19G, representing the hypothetical H1/H19G peptide mixture. These spectra predict that the amount of  $\beta$ -sheet and random coil would increase slightly with increasing temperature if the two peptides were not interacting.

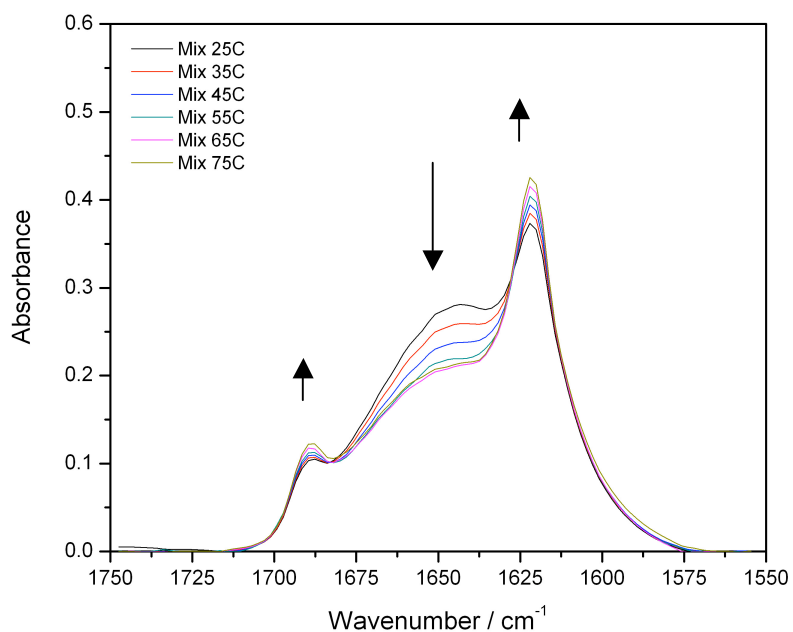


**Figure 15.** Absorbance spectra for the H1/H19G peptide mixture, which was more concentrated in H1 than in H19G. The amount of  $\beta$ -sheet increased and the amount of random coil decreased as temperature increased.

This experiment was repeated to test the reproducibility of the results. Figures 16 and 17 present IR temperature dependence spectra of H1 and H19G from the second trial. As expected, the H1 spectra revealed  $\beta$ -sheet secondary structure, and the H19G spectra revealed random coil structure. As before, the amount of each type of structure increased as the temperature was increased.

Integration of the two peptides' amide I' bands revealed that the H1 ( $\beta$ -sheet) solution was now more dilute than the H19G (random coil) solution. A 1:1 (by volume) mixture of these peptide solutions would therefore contain more random coil than  $\beta$ -sheet.

The spectra averaging the H1 and H19G spectra (Figure 18) predicted that if the peptides were not interacting, a combination of the two peptides would show mostly random coil structure with some  $\beta$ -sheet. Both types of secondary structure would be expected to become more abundant as the temperature increases.

When the two peptide solutions were mixed and monitored with IR, the spectra presented in Figure 19 were obtained. These spectra displayed mostly random coil structure with some  $\beta$ -sheet, in agreement with the prediction of the average spectra. Yet once again, the amount of  $\beta$ -sheet structure increased and the amount of random coil decreased drastically as the temperature was increased.

In each trial of the experiment, the peptide mixture was monitored with IR over a range of increasing temperatures from 25 °C to 75 °C in 10 °C increments. Once a spectrum had been obtained at 75 °C, the temperature was returned to 25

°C and a final spectrum was taken. By comparing the initial and final 25 °C spectra, information about the reversibility of the experiment is obtained.

Figures 20 and 21 present an overlay of the initial and final 25°C spectra for the first and second trial of the experiment, respectively. The initial and final spectra in each figure are very different from one another, so the process was irreversible in both cases. In each figure, the initial spectrum contained significant amounts of both  $\beta$ -sheet and random coil. The final spectrum, in contrast, showed that there had been a significant increase in the amount of  $\beta$ -sheet and an even larger decrease in the amount of random coil during the experiment.

Figures 20 and 21 also highlight the important observation that changes in relative concentrations did not seem to affect the overall process. Despite the fact that the relative concentrations of the two peptides were switched from the first trial to the second, the process followed the same trends of increasing  $\beta$ -sheet and decreasing random coil with increasing temperature in both trials.

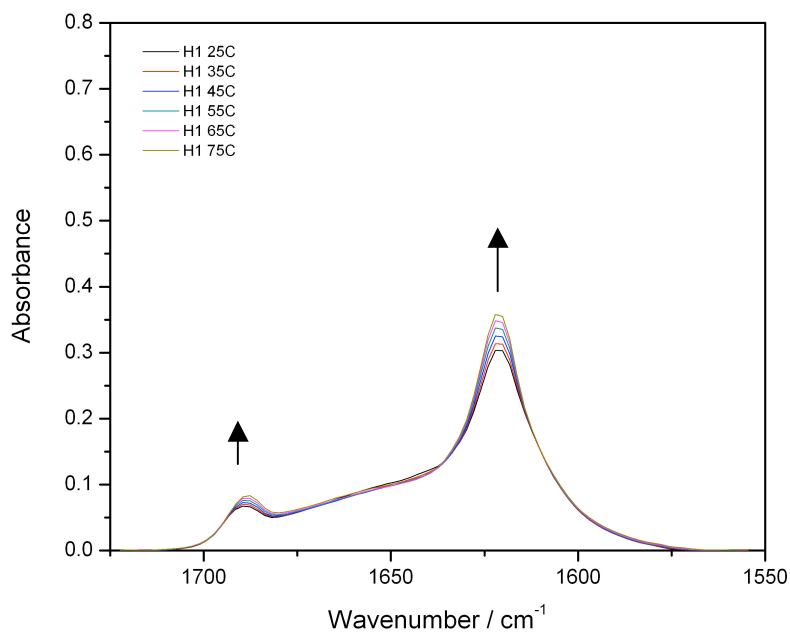


**Figure 16.** IR absorbance spectra for the more dilute H1 solution. Peaks at 1620 and 1690 cm<sup>-1</sup> reveal  $\beta$ -sheet secondary structure. The amount of  $\beta$ -sheet increased with increasing temperature.

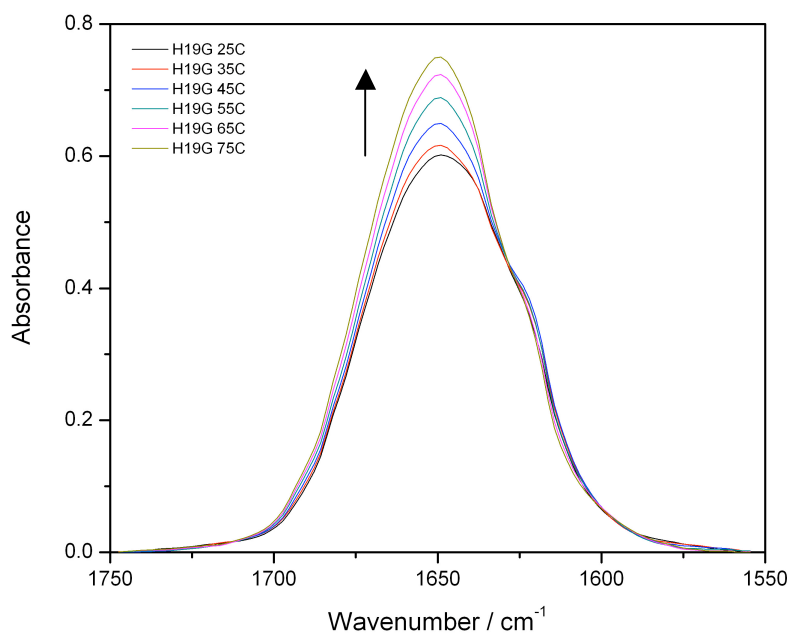


**Figure 17.** IR absorbance spectra for the more concentrated H19G solution. The broad peak at 1650 cm<sup>-1</sup> reveals the presence of random coil structure, which increased in abundance as the temperature was increased.

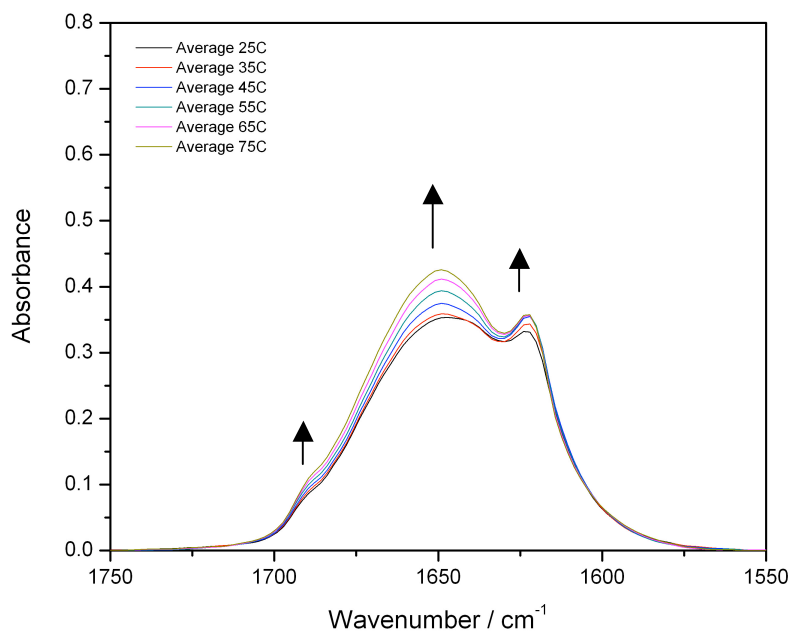


**Figure 18.** Spectra obtained by averaging the spectra of dilute H1 and concentrated H19G, representing the hypothetical H1/H19G peptide mixture. Results predict that the amount of  $\beta$ -sheet and random coil would increase slightly with increasing temperature if the two peptides were not interacting.

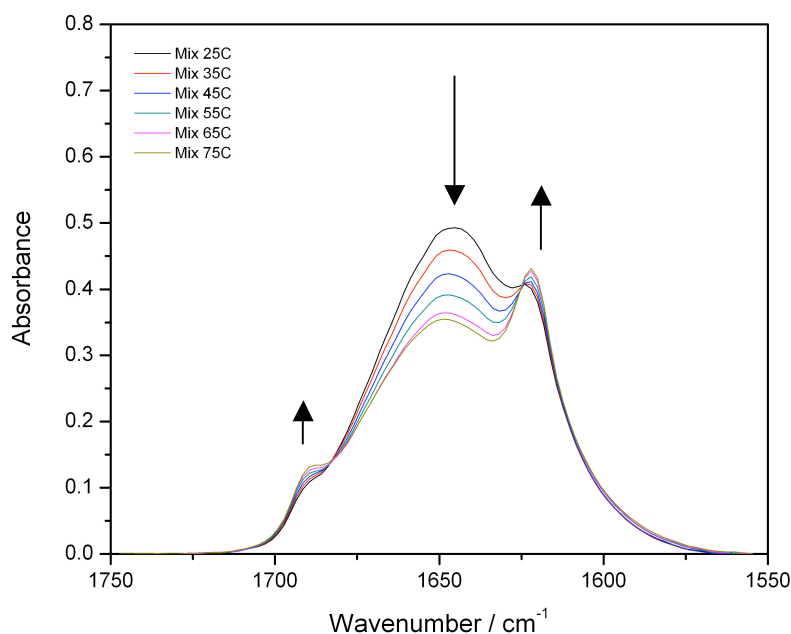


**Figure 19.** Absorbance spectra for the H1/H19G peptide mixture, which was more concentrated in H19G than H1. The amount of  $\beta$ -sheet increased and the amount of random coil decreased with increasing temperature.

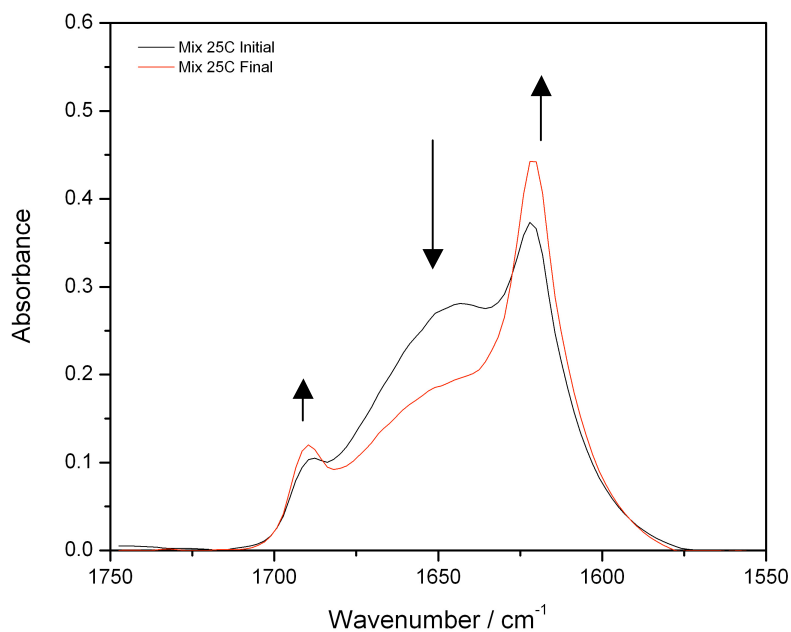


**Figure 20.** Initial and final spectra taken at 25 °C for the mixture of concentrated H1 and dilute H19G. During the experiment, the amount of  $\beta$ -sheet increased and the amount of random coil decreased. Since these spectra do not overlay, the process was irreversible.

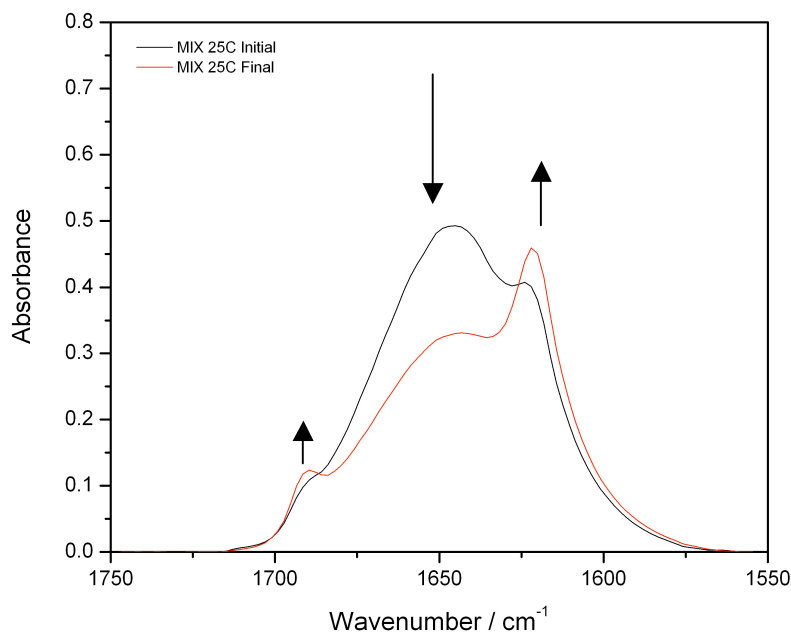


**Figure 21.** Initial and final spectra taken at 25 °C for the mixture of dilute H1 and concentrated H19G. The amount of  $\beta$ -sheet increased and the amount of random coil decreased over the course of the experiment. Since the spectra do not overlay, the process was irreversible.

### *Time and Temperature Dependence of the H1/H19G Peptide Mixture*

The results from the temperature dependence experiments did not include enough information to determine whether the observed process was a result of changing the temperature or simply the passage of time. To address this question, an experiment was designed that would allow us to separate the changes in absorbance due to time from those due to increasing temperature. A 1:1 (concentration) H1/H19G peptide mixture was monitored on three separate IR spectrometers simultaneously, where the temperature was set to a different value on each and held constant over the course of the experiment. Measurements were taken every half hour for 24 hours.

The three absorbance plots in Figure 22 show the results of this experiment. Each plot shows the absorbance changes in the amide I' region over time for the peptide mixture at either 25 °C (left panel), 35 °C (middle panel), or 45 °C (right panel). Although measurements were taken every half hour, spectra were only plotted for every fifth measurement to retain clarity.

These spectra reveal that the secondary structure of the peptide mixture was primarily  $\beta$ -sheet, with some random coil. As time passed, the amount of  $\beta$ -sheet increased and the amount of random coil decreased. These results were analogous to the changes that were observed with increasing temperature in the temperature dependence experiments. However, the decrease in random coil appeared similar in magnitude to the increase in  $\beta$ -sheet, which was not the case in the temperature dependence experiments.

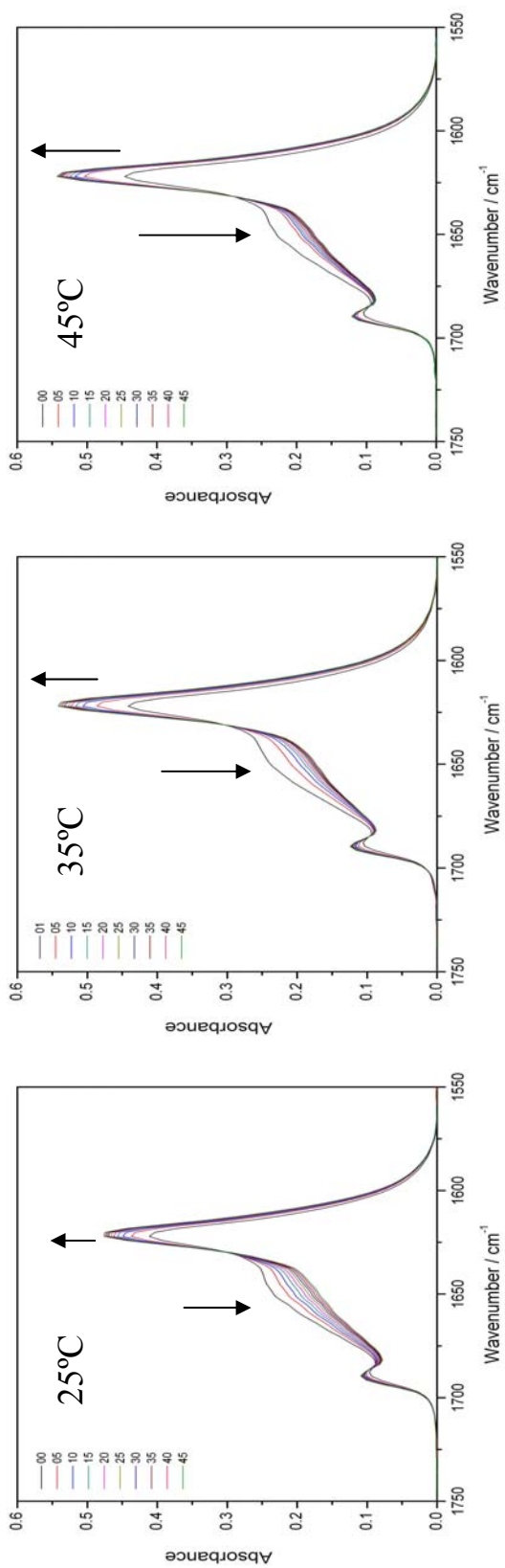


**Figure 22.** IR absorbance plots showing the time and temperature dependence of the H1 and H19G mixture. Over time (within each plot), the mixture gained  $\beta$ -sheet and lost random coil. As the temperature was increased (across the three plots), the amount of  $\beta$ -sheet formed was increased, and the process happened more quickly.

Information about the temperature dependence of the process was obtained by comparing measurements that were collected on the three different spectrometers at the same point in time. The results show that at each point in time, the amount of  $\beta$ -sheet was greater for higher temperatures. The experiment that tested the effects of both time and temperature had produced the same results for temperature dependence as the simple temperature dependence experiment.

The difference between the first and second spectra in each plot was much larger than the difference between any other adjacent spectra, which suggested that changes were happening much more rapidly at the beginning of the process. This discrepancy became more exaggerated as the temperature was increased. To better understand these trends, the data for each temperature were displayed as a kinetics plot (Figure 23) by plotting the absorbance at  $1620\text{ cm}^{-1}$  (amount of  $\beta$ -sheet) as a function of time; these plots were normalized in order to facilitate the direct comparison between each temperature's kinetics.

Using a single exponential to fit these plots resulted in a terrible fit of the data. A double exponential was needed to obtain an acceptable fit, which revealed that there were two processes occurring. The two lifetimes for each temperature were extrapolated from the fit and are presented in the table inset in Figure 23. The first process ( $T_1$ ) was short, lasting approximately one to two hours. The second process ( $T_2$ ) was longer, lasting for eight to ten hours. Comparing the lifetimes for different temperatures revealed that  $T_1$  became faster

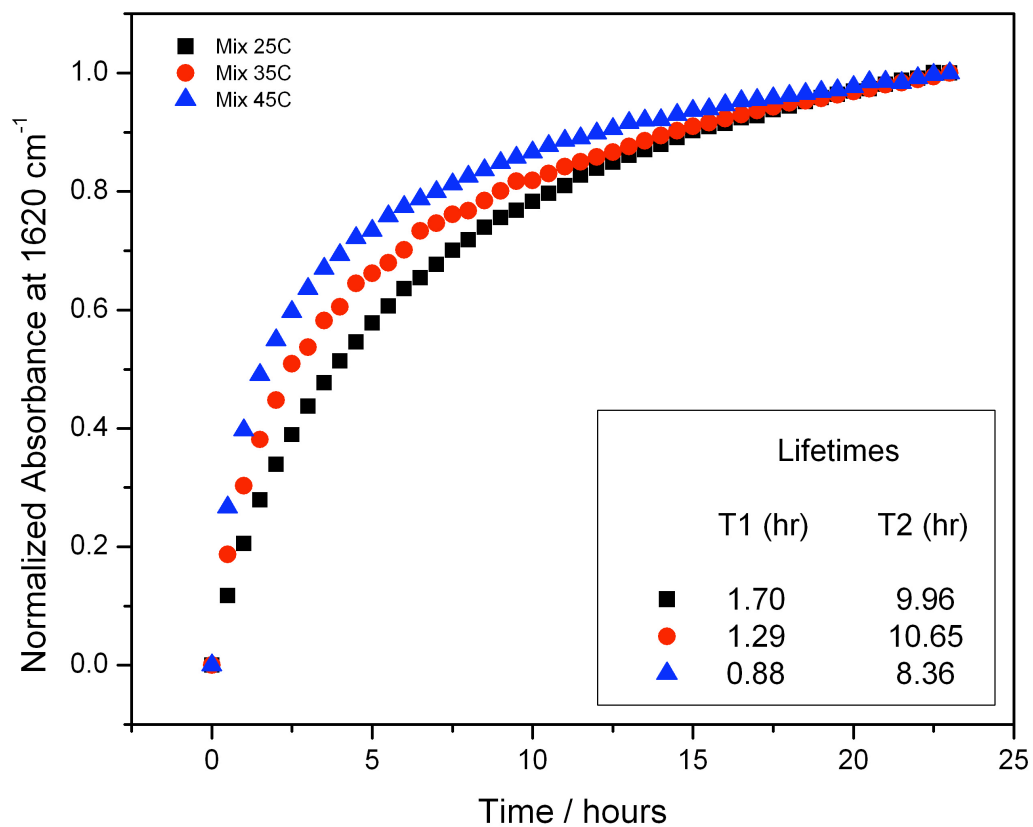


**Figure 23.** Normalized kinetics plots for the H1 and H19G peptide mixture at 25 °C, 35 °C, and 45 °C. Each plot was fitted with a double exponential function, which revealed that there were two processes occurring. Lifetimes of these processes were extrapolated from the fitted curves and are presented in the inset table. The shorter process (T1) followed Arrhenius kinetics, where the process occurred more quickly as the temperature was increased. The longer process (T2) did not follow any noticeable pattern of temperature dependence.

as the temperature was increased, but  $T_2$  did not follow an identifiable pattern of temperature dependence.

A process that becomes faster as the temperature is increased is said to follow Arrhenius kinetics. This type of process can be further analyzed through the use of an Arrhenius plot, which plots the natural logarithm of the rate constant as a function of the inverse of the temperature. For each temperature, the rate constant for the first process ( $k_1$ ) was derived from the lifetime ( $T_1$ ) using the relationship  $k_1 = \frac{1}{T_1}$ .

When kinetics data for a process that follows Arrhenius behavior is plotted in this manner, a straight line is generated that can be described by the equation  $\ln(k_1) = \frac{-E_a}{R} \left(\frac{1}{T}\right) + \ln(A)$ . In this equation,  $k_1$  is the rate constant,  $E_a$  is the activation energy of the process,  $R$  is the gas constant ( $8.314 \text{ J/mol}^1\text{K}^{-1}$ ),  $T$  is the temperature (in K), and  $A$  is a constant known as the constant of proportionality.

An Arrhenius plot was created for the H1/H19G peptide mixture kinetics and is presented in Figure 24. The line of best fit for these points was determined to be  $y = -3116.4x + 9.9012$ . This equation fits the data reasonably well, with an  $R^2$  value of 0.9875. The slope from this equation, -3116.4, was set equal to the slope given in the Arrhenius equation, which is  $\frac{-E_a}{R}$ . Substituting the value of the gas constant allowed for  $E_a$  to be calculated as 25.9 kJ/mol.

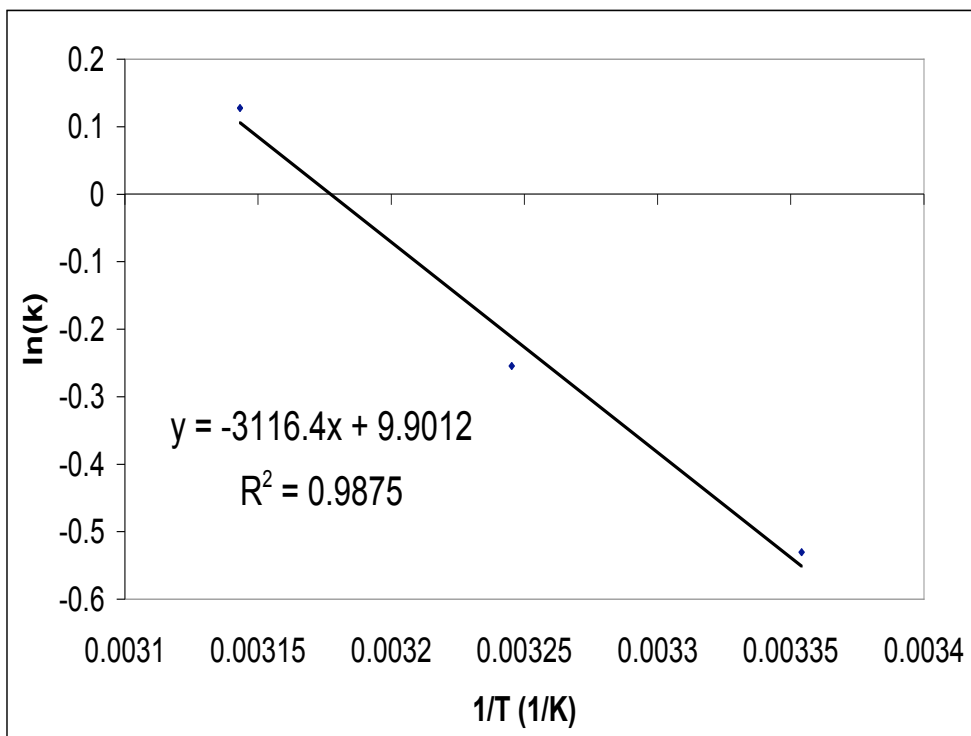


**Figure 24.** Arrhenius plot for the short process (T1), obtained by plotting the natural logarithm of the rate constant as a function of the inverse of the temperature. These data were well fit ( $R^2=0.9875$ ) by the equation  $-3116.4x+9.9012$ . Comparing the slope derived from this equation with the Arrhenius equation, written as  $\ln(k_1) = \frac{-E_a}{R} \left(\frac{1}{T}\right) + \ln(A)$ , allowed for the activation energy  $E_a$  to be calculated as 25.9 kJ/mol.

*Temperature Dependence of H1, H19G\*, and H1/H19G\* Peptide Samples*

Temperature dependence IR spectra of H1 and H19G\* are presented in Figures 25 and 26. As expected, the H1 spectrum featured the characteristic  $\beta$ -sheet bands at 1620 and 1690  $\text{cm}^{-1}$ , while the spectrum for H19G\* featured the random coil band at 1650  $\text{cm}^{-1}$ . The H19G\* spectra differed from the H19G spectra in the small band that appeared at 1600  $\text{cm}^{-1}$ , which corresponds to the vibration of the labeled backbone carbonyl. Integration of the amide I' bands for the two peptides showed that the H19G\* solution was more concentrated than the H1 solution.

Figure 27 presents the spectra that would be expected of a hypothetical 1:1 mixture of the H1 and H19G\* samples, obtained by the same method as the hypothetical H1/H19G spectra in Figure 14. The spectra show that the structure would be primarily random coil with some  $\beta$ -sheet, and that the amount of each type of structure would increase with increasing temperature.

The H1 and H19G\* peptide solutions were then combined in a 1:1 (volume) mixture and monitored over a range of temperatures with IR spectroscopy, which produced the spectra in Figure 28. In agreement with the predictions of the average spectra, these spectra revealed that the structure was mostly  $\beta$ -sheet with some random coil. They also showed that the amount of  $\beta$ -sheet increased and the amount of random coil decreased drastically as the temperature was increased, as was seen in all other temperature dependence

spectra of mixed H1 and H19G. The new peak at  $1600\text{ cm}^{-1}$  also increased in intensity with increasing temperature.

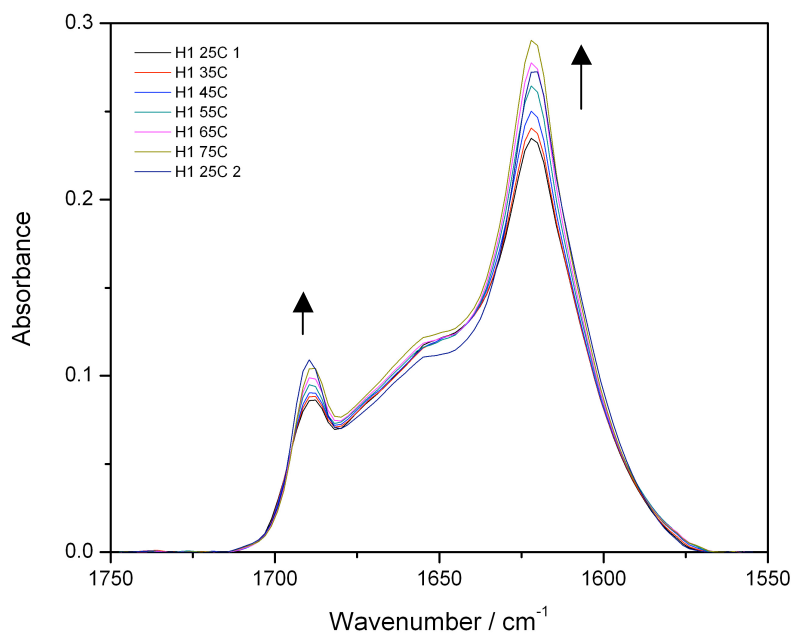


**Figure 25.** IR absorbance spectra for the H1 peptide. Peaks at 1620 and 1690  $\text{cm}^{-1}$  reveal  $\beta$ -sheet secondary structure. The amount of  $\beta$ -sheet increased with increasing temperature.

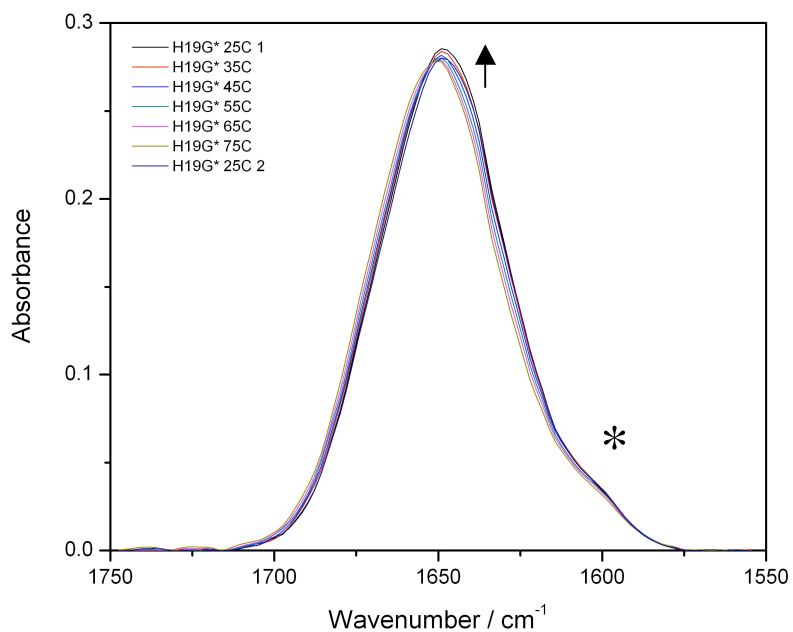


**Figure 26.** IR absorbance spectra for H19G\*. The peak at 1650  $\text{cm}^{-1}$  reveals that the secondary structure is random coil. A trace of a new peak appears at 1600  $\text{cm}^{-1}$  (noted with an asterisk), created by the vibration of the  $^{13}\text{C}$ -labeled backbone carbonyl.

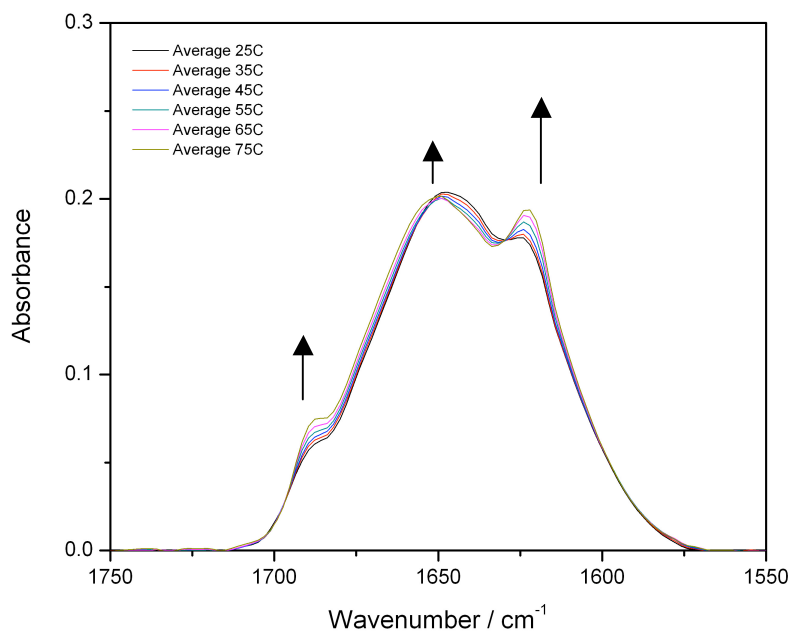


**Figure 27.** Spectra obtained by averaging the spectra of H1 and H19G\*, representing the hypothetical H1/H19G\* peptide mixture. Results predict that the amount of  $\beta$ -sheet and random coil would increase slightly with increasing temperature if the two peptides were not interacting.

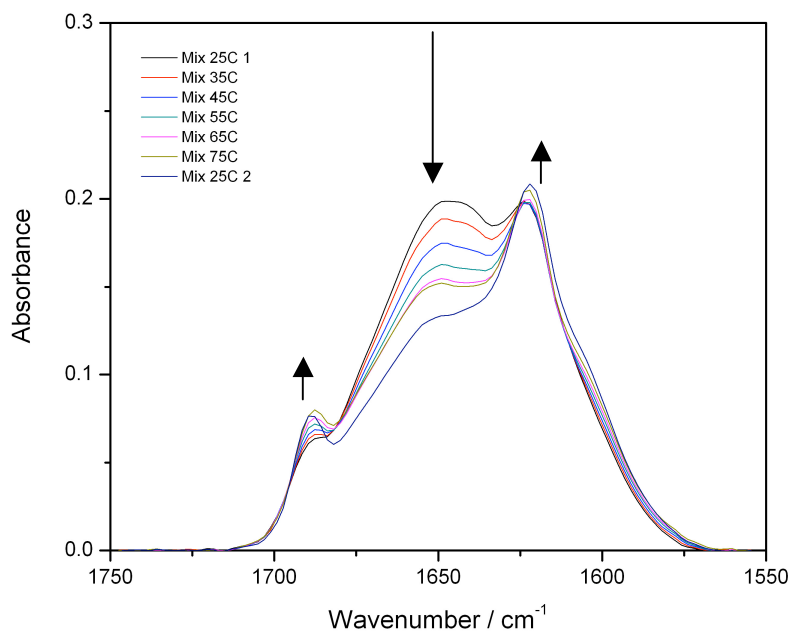


**Figure 28.** Absorbance spectra for the H1/H19G\* peptide mixture. The amount of  $\beta$ -sheet increased and the amount of random coil decreased with increasing temperature.

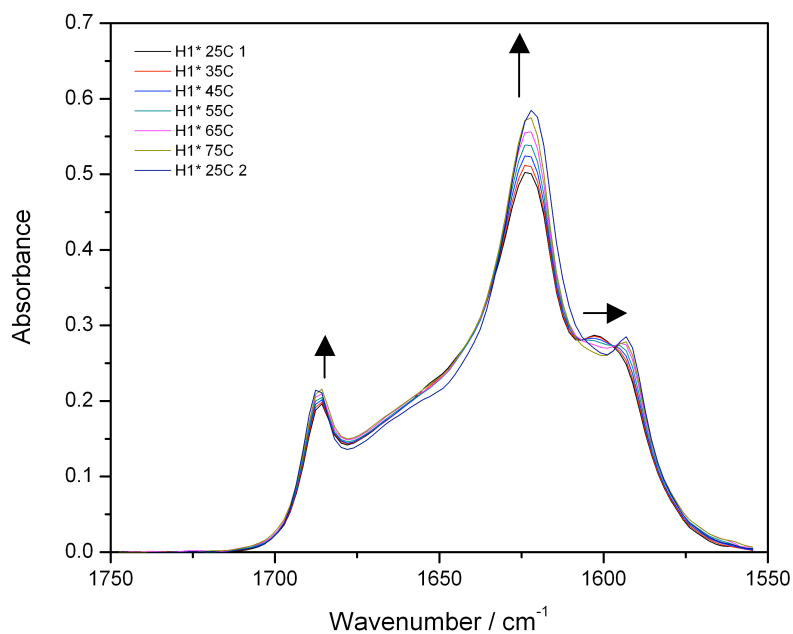
*Temperature Dependence of H1\*, H19G, and H1\*/H19G Peptide Samples*

IR spectra for H1\* and H19G at varying temperatures are presented in Figures 29 and 30. The spectra for H1\* showed characteristic  $\beta$ -sheet bands at 1620 and 1690  $\text{cm}^{-1}$ , but there was also a new band that appeared first at 1600  $\text{cm}^{-1}$  and then shifted toward 1590  $\text{cm}^{-1}$  as the temperature was increased. This additional  $\beta$ -sheet band is created by the vibration of the  $^{13}\text{C}$ -labeled backbone carbonyl. Spectra for H19G showed the characteristic random coil band at 1650  $\text{cm}^{-1}$ . As the temperature was increased, the amount of each peptide's natural secondary structure was increased. Integration of the amide I' bands of the two peptides revealed that the H19G solution was more concentrated than the H1\* solution.

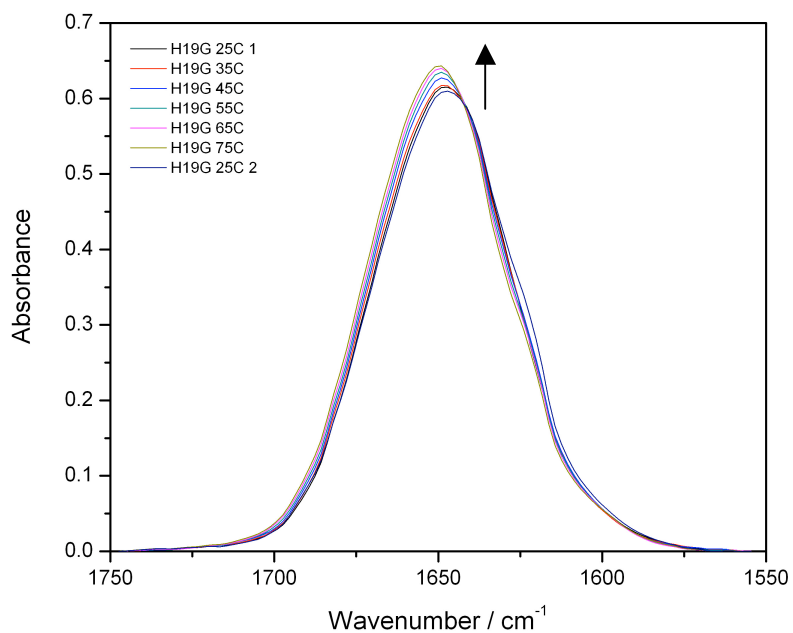
The average of the H1\* and H19G spectra are presented in Figure 31, representing a mixture of the two peptide solutions in which the two peptides did not affect one another. Figure 31 shows that this type of mixture would be expected to be mostly random coil in structure, with some  $\beta$ -sheet present (shown as bands for both the  $^{12}\text{C}$  and the  $^{13}\text{C}$   $\beta$ -sheet backbone carbonyl vibrations). As the temperature is increased, the amounts of both  $\beta$ -sheet ( $^{12}\text{C}$ ) and random coil would be expected to increase, but the  $^{13}\text{C}$ -labeled  $\beta$ -sheet band would be expected to decrease in magnitude and shift toward lower wavenumbers.

Figure 32 presents the spectrum that was obtained when the two peptide solutions were mixed in a 1:1 (volume) ratio and monitored with IR spectroscopy over a range of temperatures. At the lowest temperature, the structure was mostly

random coil with some  $\beta$ -sheet ( $^{12}\text{C}$  and  $^{13}\text{C}$ ) present. As the temperature was increased, the amount of  $\beta$ -sheet was increased, and the amount of random coil decreased dramatically. The final solution was mostly  $\beta$ -sheet in structure with some random coil present. However, unlike in the spectra for H1\*, the band at  $1600\text{ cm}^{-1}$  only increased in magnitude and did not shift to lower wavenumbers as the temperature was increased.



**Figure 29.** Absorbance spectra for H1\*. Peaks at 1620 and 1690  $\text{cm}^{-1}$  reveal  $^{12}\text{C}$   $\beta$ -sheet structure. The peak that appears first at 1600  $\text{cm}^{-1}$  and shifts towards 1590  $\text{cm}^{-1}$  is attributed to  $^{13}\text{C}$   $\beta$ -sheet structure. Both  $\beta$ -sheet signals increased in magnitude as the temperature was increased.



**Figure 30.** Absorbance spectra for H19G. These spectra show that the amount of random coil increased slightly as the temperature was increased.

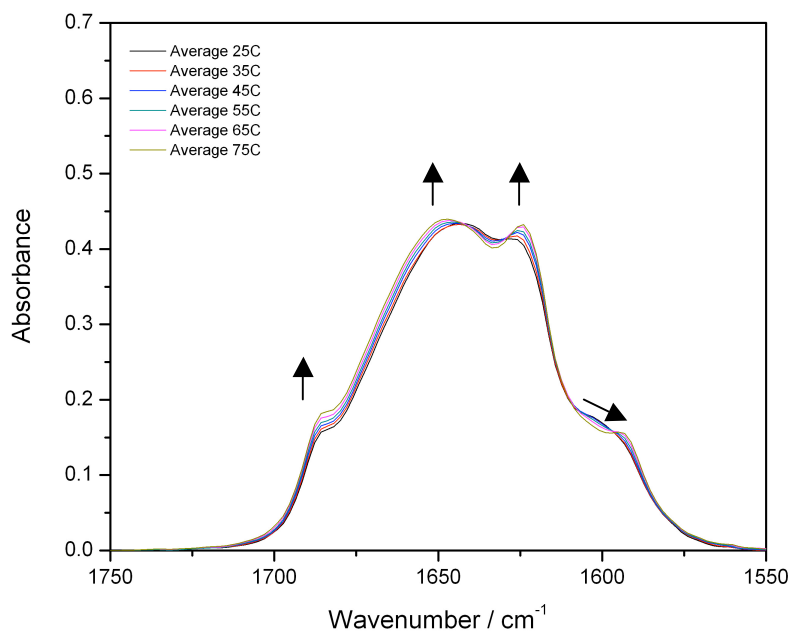


**Figure 31.** Spectra obtained by averaging the spectra of H1\* and H19G. Results predict that as the temperature is increased, the  $^{12}\text{C}$   $\beta$ -sheet and random coil bands should increase slightly, while the  $^{13}\text{C}$   $\beta$ -sheet band would be expected to decrease in magnitude and shift towards lower wavenumbers.

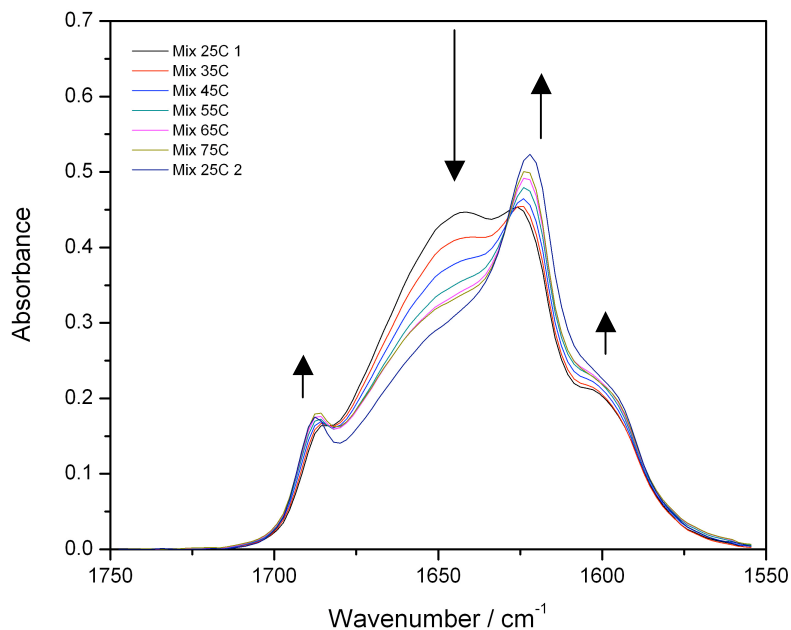


**Figure 32.** Absorbance spectra for the H1\*/H19G peptide mixture. As the temperature was increased, the amount of  $^{12}\text{C}$  and  $^{13}\text{C}$   $\beta$ -sheet increased, and the amount of random coil decreased.

*Comparison of H1/H19G\* and H1\*/H19G Temperature Dependence*

The experimental results obtained by monitoring the H1/H19G\* and H1\*/H19G peptide mixtures can also be shown as difference spectra, which are presented in Figures 33 and 34, respectively. Difference spectra are obtained by subtracting the spectrum at 25 °C from the spectra for all other temperatures. In these difference spectra, peaks that increase with increasing temperature are displayed as positive peaks, while peaks that decrease with increasing temperature are shown as negative peaks.

Figures 33 and 34 show that with either peptide labeled, the amount of  $\beta$ -sheet ( $^{12}\text{C}$  and  $^{13}\text{C}$ ) increased and the amount of random coil decreased drastically as the temperature was increased. This observation was a confirmation of observations that had already been made using the absorbance spectra in Figures 28 and 32.

The new information obtained through a comparison of the difference spectra involves insight into the growth of the  $^{12}\text{C}$  and  $^{13}\text{C}$   $\beta$ -sheet bands. Figure 33 reveals that for the H1/H19G\* mixture, the  $^{13}\text{C}$ -labeled (H19G\*)  $\beta$ -sheet band grew slightly larger than the  $^{12}\text{C}$  (H1)  $\beta$ -sheet band. In contrast, Figure 34 reveals that for the H1\*/H19G mixture, the  $^{12}\text{C}$ -labeled (H19G)  $\beta$ -sheet band increased to a dramatically larger magnitude than the  $^{13}\text{C}$  (H1\*)  $\beta$ -sheet band.

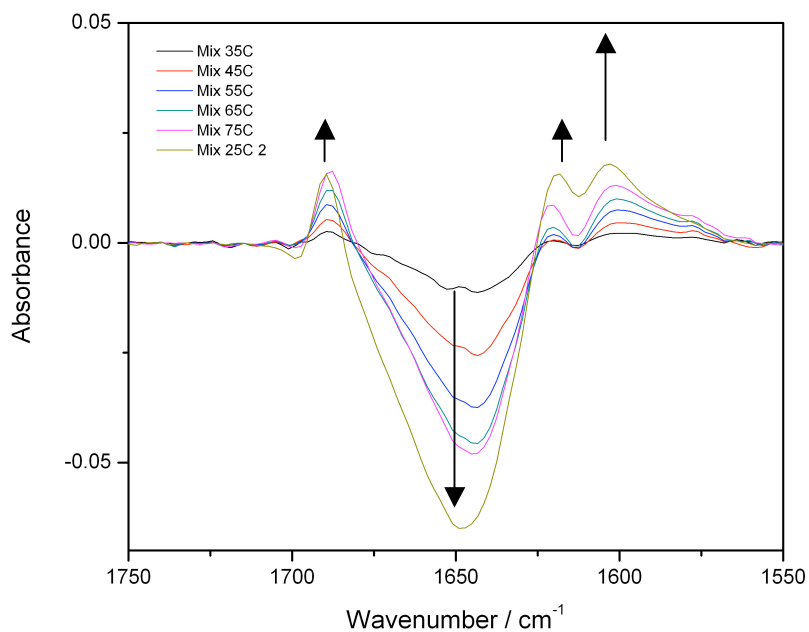


**Figure 33.** Difference spectra showing the temperature dependence of the H1/H19G\* peptide mixture. These plots reveal that the  $^{13}\text{C}$ -labeled (H19G\*)  $\beta$ -sheet band grew larger than the  $^{12}\text{C}$ -labeled (H1)  $\beta$ -sheet band.

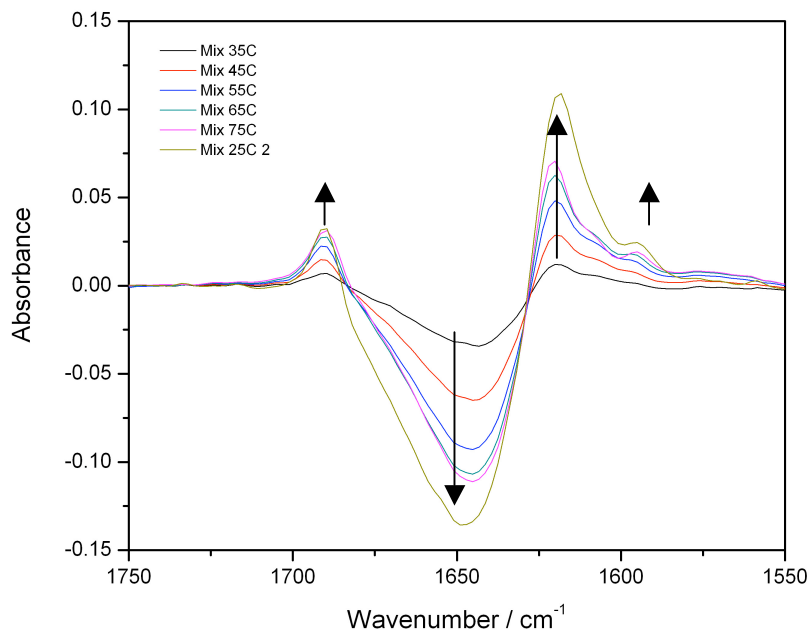


**Figure 34.** Difference spectra showing the temperature dependence of the H1\*/H19G peptide mixture. These spectra reveal that the  $^{12}\text{C}$ -labeled (H19G)  $\beta$ -sheet band increased to a larger magnitude than the  $^{13}\text{C}$ -labeled (H1\*)  $\beta$ -sheet band.

## **IV. Discussion**

### *Processing of Peptides*

Since identity and purity were confirmed for each peptide using mass spectrometry, we were confident that each solution and mixture tested contained exactly what it was supposed to contain. The observed results must then be explainable in terms of reactions of these known starting materials; the presence of contaminants or a mistaken peptide identity were eliminated as possible causes of the observed changes.

### *Temperature Dependence of H1*

IR spectra of the H1 peptide revealed antiparallel  $\beta$ -sheet secondary structure, which increased in abundance as the temperature was increased. The presence of  $\beta$ -sheet structure was unsurprising, since the H1 peptide is derived from what is thought to be the most amyloidogenic region of the Syrian hamster prion protein (PrP). However, our temperature dependence results contradicted those found by Silva, *et al.*<sup>17</sup> and Petty, *et al.*<sup>16</sup> Both authors reported that as the temperature was increased from 25 °C to 75 °C, the H1 peptide underwent a transition from  $\beta$ -sheet structure to a conformation with a significant random coil content. Our results, in contrast, showed that H1 gained  $\beta$ -sheet structure as the temperature was increased. This difference can be explained in terms of solvent differences.

In our polar solvent, hydrophobic interactions were the main force driving the formation of  $\beta$ -sheet.  $\beta$ -sheet formation results in the release of many water

molecules that were bound to the monomeric peptide, which increases the overall entropy of the system. There is a specific increase in the overall entropy ( $\Delta S$ ) associated with the formation of  $\beta$ -sheet. Since  $\Delta G = \Delta H - T\Delta S$ , increasing the temperature of the system gives more weight to the entropy term, and the overall Gibbs free energy is lowered. A lower energy corresponds to a more energetically favored process, so increasing the temperature makes  $\beta$ -sheet formation more favorable. This explains why we observed an increase in  $\beta$ -sheet structure as the temperature was increased.

Silva and Petty both used acetonitrile in their buffers, which made their solvents less polar than ours. Decreasing the polarity of the solvent decreases the strength of the hydrophobic interactions that drive  $\beta$ -sheet formation. The magnitude of the entropy change associated with  $\beta$ -sheet formation is also decreased, such that increasing the temperature no longer results in such a dramatic decrease in  $\Delta G$ . In these solvents, the formation of  $\beta$ -sheet became less favorable as the temperature increased, meaning that the  $\Delta G$  for the reaction must have been increased.

### *The Importance of Residue 117*

Comparing the IR spectra of H1 with the spectra for H19G revealed the importance of the identity of residue PrP 117 (residue 9 of H1). When residue 117 was alanine (H1), the peptide formed antiparallel  $\beta$ -sheet, but when it was glycine (H19G), the peptide was almost completely random coil. A small

structural change in the side chain of this residue, namely changing a methyl group to a proton, had a dramatic effect on the peptide's secondary structure.

These results featured the same trends in secondary structure as those observed by Petty *et al.*<sup>16</sup> In this paper, the difference in secondary structure between the two peptides was explained in terms of the side chain at residue 117. Shortening the side chain from a methyl group to a proton disrupted  $\beta$ -sheet formation by introducing extra flexibility into the backbone. As a result, the more flexible H19G peptide existed as random coil instead of forming  $\beta$ -sheet like H1.

#### *Temperature Dependence of H1 and H19G Mixtures*

The spectra representing the hypothetical mixtures of H1 and H19G (Figures 14 and 18) suggested that if the two peptides were not interacting, the overall secondary structure should be an even mixture of  $\beta$ -sheet and random coil, and that the amounts of both  $\beta$ -sheet and random coil would be expected to increase with increasing temperature.

Temperature dependence experiments performed with mixtures of H1 and H19G revealed experimental results that were very different from these predictions (Figures 15 and 19). Regardless of which species was more concentrated, the amount of  $\beta$ -sheet increased and the amount of random coil decreased drastically with increasing temperature. The difference in temperature dependence between our experimental results and the predictions for the hypothetical mixture ruled out the possibility that the two peptides were mixing

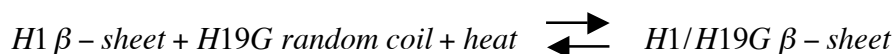
without interacting with one another. Since our results differed so greatly from these predictions, we knew the two peptides must interact when mixed. To explain our results, we suggested that the disappearing random coil (H19G) was somehow being incorporated in the  $\beta$ -sheet formed by H1.

The two trials of this experiment revealed important information regarding the concentration dependence of this process. In the first trial of this experiment, H1 was present in the mixture at a higher concentration than H19G. In the second trial, the relative concentrations of the two peptides were reversed. Yet for both trials, the same pattern of increasing  $\beta$ -sheet and decreasing random coil was observed when the temperature was increased. Changing the relative concentrations of the two peptides did not seem to affect the process. This was an important observation because we were unable to determine the concentrations of our peptide solutions before mixing them, and therefore the relative concentrations of the two peptides in the mixtures were unknown. Since we observed the same trends regardless of relative concentrations, we were able to study this process despite the difficulty of controlling the concentration in each experiment.

*The Mechanism of the Mixing Process- Thermodynamic Control*

To learn more about the mechanism of this interaction between H1 and H19G, we considered the reversibility of the process. The observed changes occurred with increasing temperature, so the reversibility of the reaction was studied with IR while increasing the temperature of the H1/H19G mix from 25°C to 75 °C and then returning it to its initial value of 25 °C. The drastic difference between the initial and final spectra taken at 25 °C (shown in Figures 20 and 21 for two trials) revealed that the observed loss of random coil and gain of  $\beta$ -sheet with increasing temperature was irreversible.

Studying reversibility allowed us to determine whether the mechanism was under thermodynamic or kinetic control. If the mixing of the two peptides were thermodynamically controlled, we would be able to write the process as the equilibrium presented below.



This equation shows that heat would be expected to act as a reactant in a thermodynamically controlled process. Increasing the temperature would perturb the equilibrium by increasing the amount of heat present in the reaction mixture.

In this case, the original equilibrium process would be the incorporation of H19G monomers into the  $\beta$ -sheet formed by H1. The disturbance would be the increased amount of heat, and the system would be expected to shift towards an increased formation of products to use up this “extra” reactant. We would

therefore expect to see an increased amount of  $\beta$ -sheet as the temperature was increased, which is what we observed in our experimental results.

However, this principle would also imply that if the temperature were then lowered, the amount of heat in the reaction mixture and the equilibrium position would be restored to their original equilibrium values. This means that as the temperature is lowered, we would expect to see a decrease in the amount of  $\beta$ -sheet as the H19G peptide returns to its random coil configuration.

The difference between the initial and final spectra in figures 20 and 21 reveals that the amount of  $\beta$ -sheet did not return to its initial value as the temperature increase was reversed. During the course of the experiment, random coil had been irreversibly incorporated into the  $\beta$ -sheet. Since the process was not reversible with respect to temperature, as we would expect for a thermodynamically controlled process, we concluded that this process was not under thermodynamic control.

#### *The Mixing Process is Under Kinetic Control*

If the mixing of the two peptides were kinetically controlled, we would be able to represent the forward process as the reaction coordinate shown in Figure 35. Since this is an equilibrium process, both the forward and reverse reactions would be occurring to some extent. The forward process would involve H1  $\beta$ -sheet and random coil H19G combining to form a  $\beta$ -sheet that contains both H1

and H19G. This figure shows that there is an activation energy barrier,  $E_a$ , which must be overcome if the reaction is to occur.

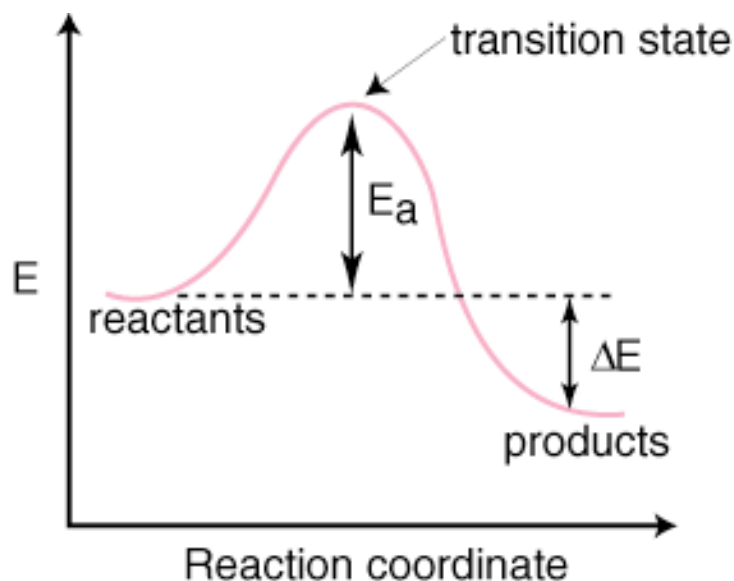


**Figure 35.** Presentation of the reaction coordinate describing a kinetically controlled process. The conversion of reactants into products has some activation barrier,  $E_a$ , which must be overcome for the reaction to occur.

We modeled the forward process as an exergonic process, where energy is released as reactants are converted to products. Exergonic processes occur spontaneously because the system is able to lower its energy and form a more energetically favorable state by reacting. The contrasting endergonic process, in which energy is required to form the H1/H19G  $\beta$ -sheet, was eliminated as a possibility because the process was observed at room temperature. Since it did not require the input of any additional energy (in the form of increasing the

temperature), we were able to conclude that it was spontaneous and therefore exergonic.

Although the process was observed at room temperature, we wanted to learn about how it was affected by changes in temperature. Increasing the temperature of the system does not change the height of the activation energy barrier, but it does increase the kinetic energy of the system. When the system has a greater kinetic energy, each possible collision of reactants has a greater probability of having enough energy to surmount the barrier and form product. If the temperature were increased, we would expect to see an increased amount of  $\beta$ -sheet and a decreased amount of random coil as more monomeric H19G was incorporated into the  $\beta$ -sheet.

As the temperature of a kinetically controlled process is decreased, the activation energy barrier remains unaffected and the kinetic energy of the system is decreased. Decreasing the system's kinetic energy reduces the probability that reactants will be able to cross the activation energy barrier to form products. Figure 35 shows that while the activation energy for the forward process is  $E_a$ , the activation energy for the reverse process must be  $E_a + \Delta E$ , where  $\Delta E$  is the energy that was released in the forward exergonic reaction. Since the activation energy for the reverse process is larger than the corresponding barrier for the forward process, it is even more unlikely that the reverse process will occur.

In this way, reducing the temperature acts to "trap" the system in the product form. A decrease in temperature would act to slow the formation of new

H1/H19G  $\beta$ -sheet, but any existing H1/H19G  $\beta$ -sheet would remain trapped in this form because the reverse reaction would be so energetically unfavorable. Decreasing the temperature of a kinetically controlled reaction should not result in a decrease in the amount of  $\beta$ -sheet observed. Therefore, a kinetically controlled process would be irreversible with respect to temperature. Since these trends are what we observed in our experimental results, we were able to conclude that the incorporation of H19G monomers into the H1  $\beta$ -sheet was a kinetically controlled process.

#### *Kinetics of the H1/H19G $\beta$ -Sheet Formation Suggest a General Mechanism*

The results from the time and temperature dependence experiments revealed that the incorporation of H19G monomers into the H1  $\beta$ -sheet occurred to an increasing extent both over time and when the temperature was increased. In other words, this is a process that occurs spontaneously but can be accelerated by increasing the temperature.

Plotting the amount of  $\beta$ -sheet (absorbance at  $1620\text{ cm}^{-1}$ ) as a function of time provided insight into how quickly the  $\beta$ -sheet was forming. We had to use a double exponential to obtain a good fit for each of these plots, which suggested the presence of two separate processes, described as  $T_1$  and  $T_2$  in the results. At this stage, it is unclear what these two processes could be, but we can get some insight from the mechanisms of fibril formation that were presented in the

introduction (Figure 5).<sup>12</sup> Our experimental results seem to be best explained by the model of templated assembly.

The model of templated assembly (see Figure 5a) describes fibril formation as the rapid binding of a preassembled nucleus to a soluble random coil peptide, followed by a rate-determining conformational change to add the peptide to the growing end of the  $\beta$ -sheet fibril. This model could provide feasible assignments of the two processes that we observed in our experiments. The H1  $\beta$ -sheet would act as the preassembled nucleus, to which the random coil H19G monomers would bind during the short  $T_1$  process. The longer  $T_2$  process would then involve the conformational change to include H19G into the growing  $\beta$ -sheet.

Other models, including monomer-directed conversion (MDC) and nucleated polymerization (NP), did not describe the mixing of H1 and H19G as well. The MDC and NP models imply that the H19G monomers are able to self-convert from their random coil conformation to adopt  $\beta$ -sheet conformation while still existing as monomers. Yet our results have not shown any indication that H19G is able to adopt a  $\beta$ -sheet conformation except when in the presence of H1. Therefore, H19G would not be able to convert to a  $\beta$ -sheet conformation until it had already associated with a  $\beta$ -sheet template or nucleus and was no longer monomeric.

### *The Magnitude of the Activation Energy*

Since the  $T_1$  process followed Arrhenius kinetics, we were able to construct an Arrhenius plot (Figure 24) and use the fit to calculate the activation energy to be 25.9 kJ/mol. This value is comparable in magnitude to the energy required to break a hydrogen bond, which is generally less than 20-25 kJ/mol.<sup>20</sup> In contrast, the energies required to break the possible covalent bonds of hydrogen, carbon, nitrogen, and oxygen are in the range of several hundred kJ/mol.<sup>21</sup> Calculating the activation energy of this process led us to conclude that the mechanism must involve the breaking of hydrogen bonds, because disrupting covalent bonds would require a much larger activation energy than what was experimentally determined.

### *Labeling Experiments Suggest a Specific Mechanism*

The amide I' band in the IR spectrum is generated by the vibrations of the backbone carbonyl. As predicted, spectra for the labeled peptides H19G\* and H1\* (Figures 26 and 29) featured a new peak around 1600  $\text{cm}^{-1}$ . This new peak arises from the vibrations of the heavier  $^{13}\text{C}$ -labeled backbone carbonyl at residue 117 (residue 9 of the H1 peptide), because changes in mass affect the frequency of vibrations.

In the IR spectrum for H19G\*, the peak for the labeled carbonyl increased in magnitude with increasing temperature in a manner that was similar to the temperature-dependent increase of the random coil band. In contrast, the

frequency of the peak for the labeled carbonyl in the H1\* spectrum shifted from  $1600\text{ cm}^{-1}$  to  $1590\text{ cm}^{-1}$ , while the unlabeled  $\beta$ -sheet bands simply increased as the temperature was increased. This shift in the band's frequency has been explained as resulting from the gradual alignment of the labeled residue 117.<sup>14</sup> As the labeled carbonyls come into alignment, they get close enough to one another to allow for strong dipole coupling, which lowers the observed frequency.

Figure 27 presented the spectra that would be expected of a mixture of H1/H19G\* in which the two peptides did not interact. Since spectra obtained from the experimental mixture of H1 and H19G\* (Figure 28) differed so greatly from these predictions, it was clear that the two peptides were interacting in some way. The experimental results followed the same trend of increasing  $\beta$ -sheet bands and the decreasing random coil band that had been observed for the H1/H19G mixtures. Therefore, we were observing the same type of process, where H19G\* monomers were being incorporated into the H1  $\beta$ -sheet.

The same conclusions were drawn for the H1\*/H19G mixture. Figure 31 showed the expected spectra of an H1\*/H19G mixture in which the two peptides did not interact. Comparing these spectra with the experimentally observed spectra for this mixture (Figure 32) revealed significant differences. The two sets of spectra were not describing the same trends, which led us to conclude that the H1\* and H19G peptides were interacting. Since the amount of  $\beta$ -sheet was increasing and the amount of random coil was decreasing (as had been observed

for all peptide mixtures), we concluded that H19G monomers were being incorporated into the H1\*  $\beta$ -sheet.

A comparison of Figures 31 and 32 also reveals an important difference in the behavior of the  $^{13}\text{C}$ -labeled carbonyl at residue 117. Figure 31 predicts that if H1\* and H19G were not interacting, the  $^{13}\text{C}$  band would be expected to decrease in magnitude and shift to lower wavenumbers. Yet Figure 32 shows that this shift was not experimentally observed. The cause of the shift in the H1\* spectra was dipole coupling between the labeled carbonyls at residue 117, so the lack of this shift in the H1\*/H19G spectra revealed that mixing these two peptides eliminated the dipole coupling between labeled carbonyls.

A lack of dipole coupling could have resulted from a loss of the registry at residue 117, but this seems unlikely. The fact that we observed the same behavior of the unlabeled  $\beta$ -sheet and random coil bands that we had seen for all other peptide mixtures suggests that we were observing the same type of process that was observed for all other peptide mixtures, which presumably included the gradual alignment at residue 117. In this case the observed process would be the inclusion of H19G monomers into the H1\*  $\beta$ -sheet.

Another way to eliminate dipole coupling would involve retaining the registry at 117, but physically blocking dipole coupling by inserting some other species between the strands of H1\*. The natural candidate for the “other species” would be the unlabeled H19G monomers.

The loss of dipole coupling suggests a more specific mechanism for the incorporation of H19G into the H1  $\beta$ -sheet. Labeled 117 residues in the H1\*  $\beta$ -strands would couple if they were adjacent to one other, so the loss of coupling (as observed through a lack of shift in frequency) implied that the H1\*  $\beta$ -strands were separated by some species, which we suggested was H19G. This observation led us to conclude that the final  $\beta$ -sheet containing both peptides must be ordered with alternating strands of H1\* and H19G, as depicted in Figure 36.

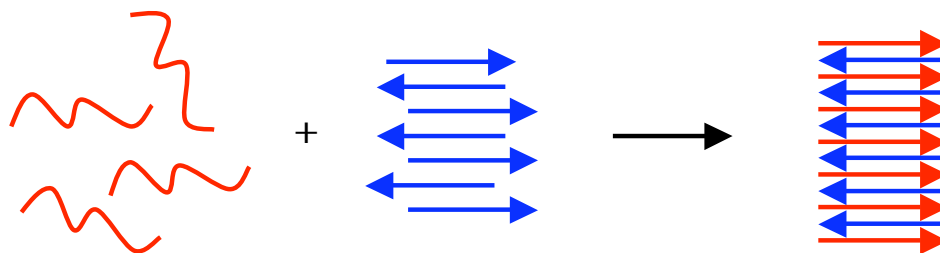


**Figure 36.** Suggested mechanism (general) of the incorporation of H19G random coil monomers (red, left) into the H1  $\beta$ -sheet (blue, center) to form a  $\beta$ -sheet containing both H1 and H19G (right).

Considering the difference spectra presented in Figures 33 (for H1/H19G\*) and 34 (for H1\*/H19G) was also instructive. The difference spectra emphasize the changes in absorbance with increasing temperature, showing increases as positive peaks and decreases as negative peaks. Spectra for both peptide mixtures featured the characteristic antiparallel  $\beta$ -sheet and random coil bands. Each set of spectra also shows a band for the vibrations of the labeled carbonyl, which exists as  $\beta$ -sheet for H19G\* (once converted) and for H1\*. For both peptide mixtures, the standard trend of increasing  $\beta$ -sheet and decreasing random coil was observed with increasing temperature. However, the two sets of spectra differ in the relative magnitudes of the in-phase unlabeled  $\beta$ -sheet band ( $1620\text{ cm}^{-1}$ ) and the band for the labeled  $\beta$ -sheet carbonyl stretch ( $1600\text{ cm}^{-1}$ ).

We were able to compare the relative growths of these two peaks to learn more about where the new  $\beta$ -sheet was coming from; possible sources included from the conversion of H19G monomers or a pool of monomeric H1. In Figure 33, the peak for the vibration of the labeled  $\beta$ -sheet carbonyl increased to a greater extent than the peak for the unlabeled  $\beta$ -sheet. These results revealed that the majority of the  $\beta$ -sheet growth was an increase in the amount of labeled  $\beta$ -sheet, which corresponded to the conformational conversion of H19G\*. This relationship was reversed in Figure 34, which shows that the peak for the vibration of the unlabeled  $\beta$ -sheet carbonyl increased much more dramatically than the peak for labeled  $\beta$ -sheet. The vast majority of  $\beta$ -sheet growth in this

experiment was an increase in the amount of unlabeled  $\beta$ -sheet, which corresponded to the conversion of H19G.

Both of these experiments showed that the increase in the amount of  $\beta$ -sheet is due to the structural conversion of H19G from random coil to  $\beta$ -sheet. In both cases, there was also a small percentage of  $\beta$ -sheet growth that was from H1 monomers adding to the  $\beta$ -sheet as well.

#### *Considering the Mixing Process in Greater Detail*

The proposed mechanism fit with what we had learned from previous experiments and allowed us to expand our prior analyses. The two processes identified from the kinetics plot of the H1/H19G mixture can be reinterpreted in light of the new mechanism. Obtaining a mixed  $\beta$ -sheet with alternating strands would be more complicated than the simple templated assembly model suggested previously. Templated assembly might still describe the first step; a single H19G monomer would be able to rapidly associate with the H1 “nucleus” in the rapid step that would correspond to  $T_1$ , and these peptides would then rearrange in the rate-determining  $T_2$  process to incorporate H19G onto the growing end of the  $\beta$ -sheet.

However, once an H19G monomer had been added onto the growing end of the  $\beta$ -sheet, there would not be any available binding sites for subsequent H19G monomers. In order for a new monomer to be able to associate with the  $\beta$ -sheet, a new  $\beta$ -sheet strand must be exposed. This process would involve the

breaking of hydrogen bonds (see Figure 37) as strands were removed from the  $\beta$ -sheet, which was identified as a necessary step of the mechanism from the magnitude of the activation energy. By the end of the process, the separated strands must recombine to form the mixed  $\beta$ -sheet described above.

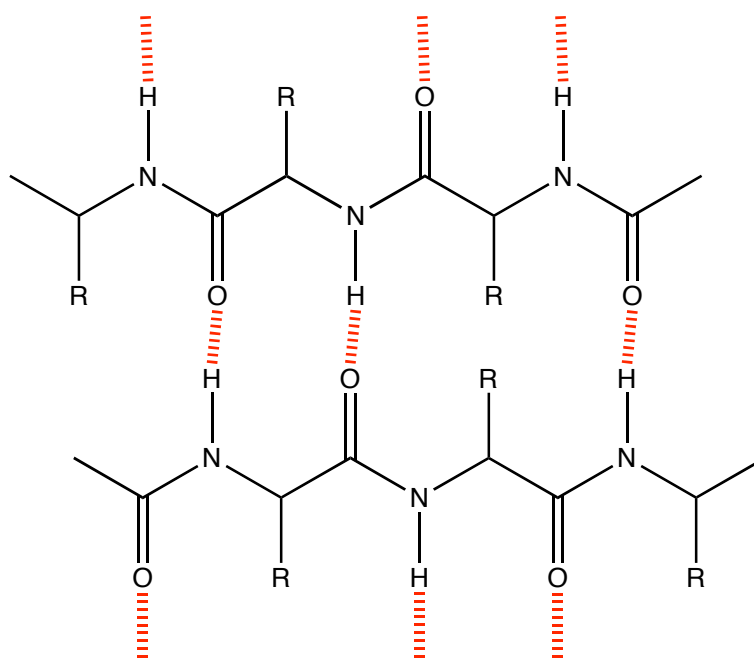


**Figure 37.** Two adjacent  $\beta$ -strands, held together by interstrand hydrogen bonding (in red). These hydrogen bonds are broken to expose new binding sites on the  $\beta$ -sheet for incoming H19G monomers. The energy required to break these hydrogen bonds is the activation energy of the mixing process.

The process of strands breaking away from the  $\beta$ -sheet and then reattaching has also been proposed by Petty to explain the mechanism of H1 alignment.<sup>15</sup> She had used isotope-edited IR spectroscopy to monitor the mixing of H1 and H1\* solutions. The IR spectra for H1\* alone featured a shift to lower wavenumbers for the <sup>13</sup>C-labeled band, which was explained by transition dipole coupling. However, spectra for the H1/H1\* mixture did not contain this shift. These results were interpreted to mean that the H1\* strands must have been separated by the unlabeled H1 strands, such that the coupling was disrupted. In order for the strands to adopt this configuration, the mechanism must involve a complete mixing of the two species. This could occur if the strands detached from the  $\beta$ -sheet and then reattached in a different order, as illustrated in Figure 38. Petty concluded that although H1 exists primarily in a  $\beta$ -sheet conformation, the H1  $\beta$ -sheet is actually in a dynamic equilibrium with monomeric H1.

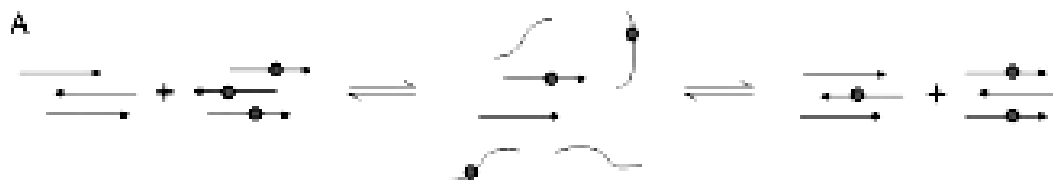


**Figure 38.** Suggested mechanism of  $\beta$ -strand alignment for the H1 peptide at low concentrations. This mechanism suggests that  $\beta$ -strands are mixed as they break away from the  $\beta$ -sheet and then reattach in a different order. Labeled residues are shown as gray circles. Figure from Petty, 2005.<sup>15</sup>

There are many parallels between Petty's results and the results that we observed in our study. We both used isotope-edited IR spectroscopy to observe a process that involved the elimination of dipole coupling, which meant that the mechanism of each process must involve a separation of the labeled strands. To explain this separation, both studies suggested a final  $\beta$ -sheet configuration that contained alternating strands of labeled H1 and some other species (unlabeled H1 or H19G). Furthermore, both studies found that the process occurred with similar activation energies (23.5 kJ/mol versus 25.9 kJ/mol, corresponding to the breaking of hydrogen bonds) and on similar timescales. The many similarities between the two processes provide strong evidence to suggest that the incorporation of H19G monomers occurs by a similar mechanism to the alignment of H1.

Figure 39a presents a summarized cartoon of the mechanism for H1 alignment. H1  $\beta$ -strands are thoroughly mixed as they break away from the  $\beta$ -sheet and reattach in a different order.<sup>15</sup> We are suggesting that this same process (depicted in detail in Figure 38) is occurring during the mixing of H1 and H19G solutions. Adding H19G increases the pool of monomers, which shifts the equilibrium towards the formation of more  $\beta$ -sheet to use up the "extra" reactant. The step involving the reattachment of H1 monomers to the  $\beta$ -sheet is simply adjusted to include the addition of the H19G monomers to the  $\beta$ -sheet during this stage (Figure 39b).

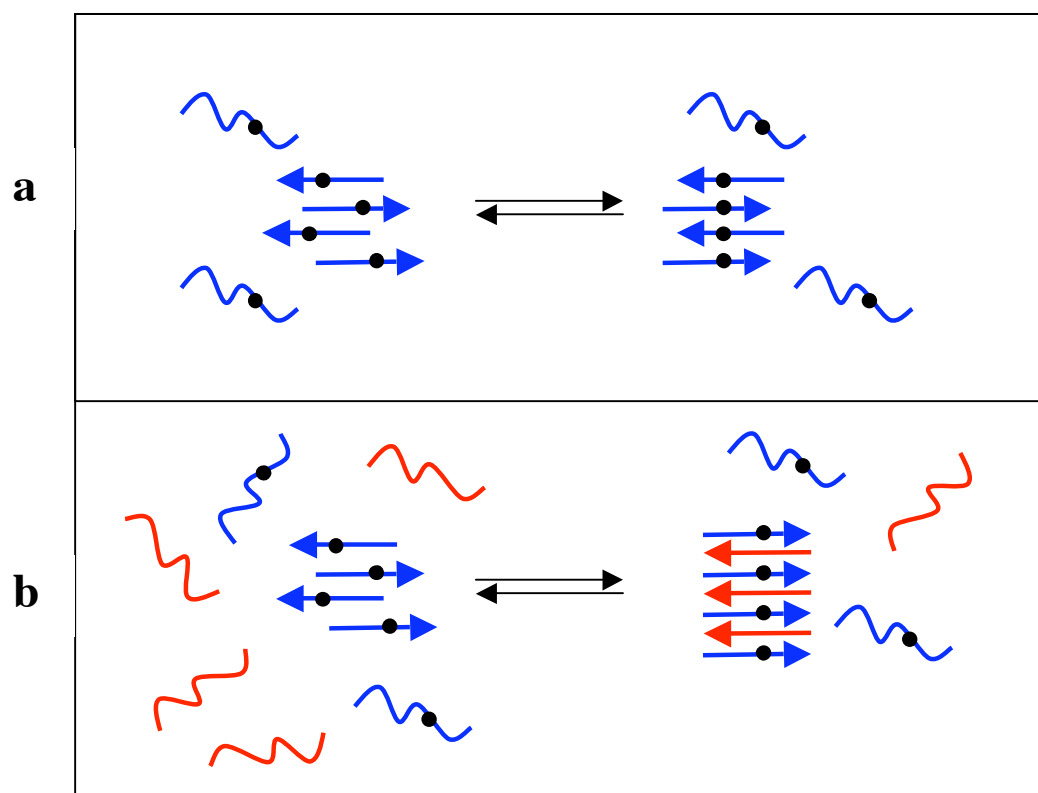


**Figure 39.** (a) The H1 peptide aligns at residue 117 by the mechanism suggested in Figure 38, involving the continuous detaching and reattaching of  $\beta$ -strands. This process results in a complete mixing of strands (b) H19G monomers may be incorporated into the H1  $\beta$ -sheet by a similar mechanism. In this case, both H19G and H1 monomers add onto the  $\beta$ -sheet. The end result is still a completely mixed  $\beta$ -sheet. Labeled residues are shown as black circles.

*The Mixing of H1 and H19G as a General Model for the Behavior of PrP*

The results from this study also provide a reasonable model for the general behavior of the parent protein, PrP. In the absence of H1, H19G monomers retain their random coil structure. Yet when H1  $\beta$ -sheet is introduced, H19G undergoes a conformational conversion to  $\beta$ -sheet structure. The presence of the H1  $\beta$ -sheet provides a template that allows for the structural conversion of H19G.

The normal form of the prion protein ( $\text{PrP}^{\text{C}}$ ) is also monomeric in structure. Once the infectious isoform (the primarily  $\beta$ -sheet  $\text{PrP}^{\text{Sc}}$ ) is introduced, however,  $\text{PrP}^{\text{C}}$  undergoes a conformational conversion to form  $\text{PrP}^{\text{Sc}}$  (see Figure 40).<sup>22</sup> Each process features a conformational change in one species (H19G and  $\text{PrP}^{\text{C}}$ ) that is induced by the provided template (H1 and  $\text{PrP}^{\text{Sc}}$ ). The end result is the formation of more of the  $\beta$ -sheet template species, so that the overall process is an autocatalytic conversion.

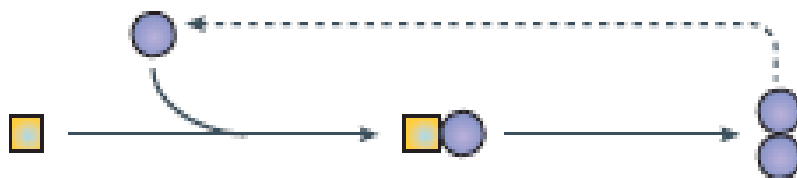


**Figure 40.** Introducing the infectious isoform  $\text{PrP}^{\text{Sc}}$  (purple circle) to the normal  $\text{PrP}^{\text{C}}$  protein (yellow square) results in the conversion of  $\text{PrP}^{\text{C}}$  to  $\text{PrP}^{\text{Sc}}$ .  $\text{PrP}^{\text{C}}$  first associates with  $\text{PrP}^{\text{Sc}}$  and then rearranges to assume the  $\text{PrP}^{\text{Sc}}$  conformation, resulting in a  $\text{PrP}^{\text{Sc}}$  dimer. Figure adapted from Weissmann, 2004.<sup>22</sup>

There is a long list of diseases that are caused by protein misfolding and aggregation, but TSEs are unique because they are transmissible.<sup>23</sup> This feature of the TSEs makes sense in light of the behavior described above. The normal form of the prion protein is present in all hosts, but the introduction of the misfolded infectious isoform seeds the conversion of normal PrP<sup>C</sup> to PrP<sup>Sc</sup>. It is in this manner that the infectious prions replicate in organisms.

Introduction of PrP<sup>Sc</sup> can occur in many ways. It is thought that bovine spongiform encephalopathy (BSE) originated from the practice of incorporating processed animal meat and bone meal into feed, which was a low-cost way to provide a high-protein diet. Initially, the cows might have been fed remains of sheep that had died of scrapie, which is another TSE. The infectious prions that had killed the sheep would then be ingested by the cow. Once in the body, these prions would seed the conformational conversion (described above) of the cow's normal prion proteins, which would result in pathogenesis in the cow. This cycle would then be repeated, as each cow that died would be incorporated into the feed for the other cows in the herd.

Transmission can occur within a species, as observed with the transfer of BSE throughout a herd. Another example of inter-species transmission is the human disease Kuru, which is associated with cannibalistic feasts. Kuru is transferred through the ritualistic consumption of contaminated human flesh.

However, an important feature of prion diseases is that there does not seem to be an absolute species barrier. PrP<sup>Sc</sup> is thought to have been introduced to

cows from the practice of feeding them contaminated sheep remains. Similarly, humans have contracted BSE by eating contaminated beef.<sup>24</sup> It is clear that the infectious agent from one species can act as a template to seed the conversion of the normal protein of another species.

Another method of introducing the infectious prion could be through genetic mutations. This is thought to be the cause of the human Creutzfeldt-Jakob disease. A mutation in the prion protein could make the spontaneous conversion from PrP<sup>C</sup> to PrP<sup>Sc</sup> more likely, and PrP<sup>Sc</sup> could then convert the remaining PrP<sup>C</sup> as described above.<sup>24</sup>

In all cases, the seeding mechanism that we observed with H1 and H19G mixtures seems to apply to the infectious and normal isoforms of the prion protein. This is a logical extension; since H1 was derived from the prion protein, we would expect to see similar behavior. Studying these types of peptide mixtures provides useful information about the structural changes observed in the local system, but a deeper level of meaning can also be assigned by including a consideration of how this work fits into the big picture of prion disease.

## References:

1. Eisenberg, Henryk. **2002**. Macromolecular marvels. *Nature*, 415, 261-262.
2. Lodish, H.; Berk, A.; Matsudaira, P.; Kaiser, C. A.; Krieger, M.; Scott, M. P.; Zipurksy, S. L.; Darnell, J. *Molecular Cell Biology 5th ed.* WH Freeman and Company: New York, NY. 2004.
3. Dobson, Christopher M. **2003**. Protein folding and misfolding. *Nature*, 426, 884-890.
4. Anfinsen, Christian B. **1973**. Principles that Govern the Folding of Protein Chains. *Science*, 181, 223-230.
5. Alberts, Bruce; Johnson, Alexander; Lewis, Julian; Raff, Martin; Roberts, Keith; Walter, Peter. *Molecular Biology of the Cell*. New York and London: Garland Science. 2002.
6. Mayor, Ugo; Johnson, Christopher M.; Daggett, Valerie; Fersht, Alan R. **2000**. Protein folding and unfolding in microseconds to nanoseconds by experiment and simulation. *PNAS*, 97, 13518-13522,
7. Daggett, Valerie; Fersht, Alan R. **2003**. Is there a unifying mechanism for protein folding? *TRENDS in Biochemical Science*, 28, 18-25.
8. Jahn, Thomas R.; Radford, Sheena E. **2005**. The Yin and Yang of protein folding. *FEBS Journal*, 272, 5962-5970.
9. Clark, Patricia A. **2004**. Protein folding in the cell: reshaping the folding funnel. *TRENDS in Biochemical Science*, 29, 527-534.
10. Murphy, Regina M. **2002**. Peptide aggregation in neurodegenerative disease. *Annu. Rev. Biomed. Eng.*, 4, 155-174.
11. Dobson, Christopher M. **2004**. Principles of protein folding, misfolding and aggregation. *Seminars in Cell & Developmental Biology*, 15, 3-16.
12. Kelly, Jeffrey W. **2000**. Mechanisms of Amyloidogenesis. *Nature Structural Biology*, 7, 824-826.
13. Barth, Andreas; Zscherp, Christian. **2002**. What vibrations tell us about proteins. *Quarterly Reviews of Biophysics*, 35, 369-430.

14. Decatur, Sean M. **2006**. Elucidation of Residue-Level Structure and Dynamics of Polypeptides via Isotope-Edited Infrared Spectroscopy. *Accounts of Chemical Research*, 39, 169-175.
15. Petty, Sarah A.; Decatur, Sean M. **2005**. Intersheet rearrangement of polypeptides during nucleation of  $\beta$ -sheet aggregates. *PNAS*, 102, 14272-14277.
16. Petty, Sarah A.; Adalsteinsson, Thorsteinn; Decatur, Sean M. **2005**. Correlations among Morphology,  $\beta$ -sheet Stability, and Molecular Structure in Prion Peptide Aggregates. *Biochemistry*, 44, 4720-4726.
17. Silva, R. A. Gangani D.; Barber-Armstrong, Wendy; Decatur, Sean M. **2003**. The Organization and Assembly of a  $\beta$ -Sheet Formed by a Prion Peptide in Solution: An Isotope-Edited FTIR Study. *JACS*, 125, 13674-13675.
18. Grant, Gregory A. *Synthetic Peptides: A User's Guide*. Second Edition. Oxford University Press, New York. 2002.
19. Basic Steps in Solid Phase Peptide Synthesis Using Fmoc-Chemistry. <[http://www.sigmaaldrich.com/Brands/Sigma\\_Genosys/Custom\\_Peptides/Key\\_Resources/Solid\\_Phase\\_Synthesis.html](http://www.sigmaaldrich.com/Brands/Sigma_Genosys/Custom_Peptides/Key_Resources/Solid_Phase_Synthesis.html)>. Accessed March 25, 2008.
20. IUPAC Compendium of Chemical Terminology, Electronic version, <http://goldbook.iupac.org/H02899.html>. Accessed April 23, 2008.
21. Brown, Theodore L.; LeMay, H. Eugene; Bursten, Bruce E.; Burdge, Julia R. *Chemistry: The Central Science*; Pearson Education, Inc.: New Jersey, 2003.
22. Weissmann, Charles. **2004**. The State of the Prion. *Nature Reviews: Microbiology*, 2, 861-871.
23. Caughey, Byron; Baron, Gerald S. **2006**. Prions and their partners in crime. *Nature*, 443, 803-810.
24. Willesmith, John W. *Manual on Bovine Spongiform Encephalopathy*. Food and Agriculture Organization of the United Nations. Rome, 1998.